this phenotype. Although DA neurons in the SN of Parkin KO mice do not show axonal degeneration or neuronal death with age like those of AR-JP patients, there is some evidence that DA neurons in Parkin KO mice are functionally disturbed. Therefore, we expected that DA neurons in Pael-R Tg mice might be subjected to stress to deal with elevated DA content. DA neurotoxins 6-OHDA and MPTP, which have been used to develop PD animal models, behave as catecholaminergic or DA neuron-specific neurotoxins (Betarbet et al., 2002). To evaluate the vulnerability of mice with altered Pael-R expression to these neurotoxins, the number of TH-immunopositive neurons in the SN or the amounts of DA in the striatum was evaluated after the treatment. The SN of PrP-Tg and non-Tg littermates that were treated with 6-OHDA-injection into the left striatum showed, respectively, 64% and 16% reduction of TH-immunopositive neurons compared with the untreated hemisphere (Fig. 5B and C). In contrast, MPTP-treatments of WT and Pael-R KO mice led to 27% and 4% fewer TH-immunoreactive neurons, respectively, than counted in saline-treated WT mice (Fig. 5D and E). The amount of striatal DA in Pael-R KO mice and WT littermates 3 weeks after 6-OHDA-injection into the left striatum showed, respectively, 38% and 81% reduction compared with the untreated hemisphere (Fig. 5F). These results indicate that DA neurons in PrP-Tg mice are more sensitive to DA neurotoxins, suggesting that these DA neurons are potentially stressed. Conversely, DA neurons in Pael-R KO mice appeared to be less sensitive (i.e., to have the opposite characteristics from that in PrP-Tg mice).

3.6. Electrophysiological analysis of DA neurons in Pael-R-KO and PrP-Tg mice

To study how the function of DA neurons was influenced by the expression of Pael-R, we made the whole-cell patch-clamp recordings from DA neurons in midbrain slices and slices containing the striatum prepared from Pael-R KO and PrP-Tg mice of postnatal 3–4 weeks. In both DA neurons of Pael-R KO (WT, n = 36 cells, KO, n = 39 cells) and PrP-Tg (non-Tg, n = 28 cells, Tg, n = 28 cells) mice we found no changes in the resting membrane potentials (WT, -55.4 ± 0.8 mV, KO, -55.0 ± 0.7 mV; non-Tg, -57.2 ± 0.9 mV, Tg, -55.3 ± 1.2 mV), the spike thresholds (WT, -30.0 ± 0.5 mV, KO, -29.8 ± 0.6 mV; non-Tg, -29.5 ± 0.5 mV, Tg, -30.4 ± 0.4 mV), the peak values (WT, 26.9 ± 1.1 mV, KO, 26.8 ± 1.1 mV; non-Tg, 27.8 ± 1.3 mV, Tg, 27.3 ± 1.3 mV), and amplitudes (WT, 56.9 ± 1.0 mV, KO, 56.6 ± 1.3 mV; non-Tg, 57.4 ± 1.2 mV, Tg, 57.6 ± 1.3 mV) of action potentials, the spike widths at half amplitude (WT, 1.46 ± 0.05 ms, KO, 1.47 ± 0.06 ms; non-Tg, 1.57 ± 0.06 ms, Tg, 1.53 ± 0.06 ms), spontaneous firing frequencies (WT, 2.87 ± 0.20 Hz, KO, 2.50 ± 0.20 Hz; non-Tg, 1.85 ± 0.13 Hz, Tg, 1.81 ± 0.15 Hz), and firing patterns. However, the input resistance of DA neurons of PrP-Tg mice

was slightly larger (Student's t-test, $P < 0.05$; Fig. 6A) than that of the non-Tg control neurons although there was no difference between DA neurons of Pael-R KO and WT mice (data not shown). Interestingly, the input resistance in the striatal MSNs was smaller in Pael-R KO mice (WT, n = 16, 133.3 ± 18.9 MΩ; KO, n = 14, 57.6 ± 9.8 MΩ, $P < 0.01$) and larger in PrP-Tg mice (non-Tg, n = 19, 81.9 ± 22.3 MΩ; Tg, n = 22, 146.2 ± 21.4 MΩ, $P < 0.05$) than their respective controls (data not shown). Since the factors which determine the input resistance are the cell size and the density and permeability of various types of ion channels incorporated into the cell membrane, our finding that the cell size of the Tg DA neurons was similar to that of non-Tg controls (soma area: non-Tg, 303 ± 14 μm^2, n = 29; Tg, 286 ± 16 μm^2, n = 26; $P > 0.4338$) suggests a possible interaction of Pael-R with a certain membranous component.

Electrical stimulation of cortico- and nigro-striatal pathways in striatal slices evokes release of DA from the residual dopaminergic nerve terminals (Calabresi et al., 1995). The released DA then depresses GABAergic IPSC in the striatal MSNs by activation of presynaptic DA D2 receptors (Bamford et al., 2004; Centonze et al., 2002, 2003, 2004). We thus performed paired pulse stimulation to get paired pulse ratios (PPRs) of the second IPSC amplitudes to the first in the MSN to study a change in DA release in Pael-R KO and PrP-Tg mice. We found no statistical change in PPRs in both Pael-R KO and PrP-Tg mice with respect to their respective controls (upper left in Fig. 6B, and data not shown). Nomifensine is a selective DA uptake inhibitor interacting with the DA transporter at a site different from that of cocaine. A previous report demonstrated that both cocaine and amphetamine, more potent drugs than nomifensine, increased the DA content and suppressed IPSCs through activation of presynaptic DA D2 receptors (Centonze et al., 2002; Wieczorek and Kruk, 1994). After nomifensine application there was a slight increase in PPR in WT and a decrease in KO at an interval of 100 ms, yielding a significant difference only in Pael-R KO mice (lower left in Fig. 6B, $P < 0.05$). Furthermore, we found a significant decrease in IPSC amplitudes upon repeated low frequency stimulation (30 pulses applied 70 ms apart) both before and after application of nomifensine in Pael-R KO mice (right in Fig. 6B). In contrast, no change was observed in PPRs and IPSC amplitudes with paired pulse stimulation and repeated low frequency stimulation before and after nomifensine in PrP-Tg mice (data not shown). In both types of mice there were no changes in rise time and decay time constant of IPSC, suggesting no alterations in GABA$_A$ receptor channel kinetics *per se* (data not shown).

These results suggest that in Pael-R KO mice DA is significantly less released while electrophysiological properties of DA neurons remain unchanged. On the other hand, we did not observe any significant changes in DA neurons of PrP-Tg mice except for a small increase in input resistance probably because

---

MPTP-treated (+) or saline-treated (−) brains containing the SN are shown. (F) Effect of 6-OHDA on DA neurons of Pael-R KO mice. 6-OHDA was injected as in B at 2–3 months of age. The amount of DA in the striatum was measured by HPLC-EC method 21 days after administration. To correct for genotype-based differences in the amount of striatal DA, data are represented as percentage of the amount on the non-treated side (right striatum) of each animal (mean $\pm$ S.E.M., Tg, n = 5; non-Tg, n = 5). ***$P < 0.001$ vs. non-Tg by Student's t-test.
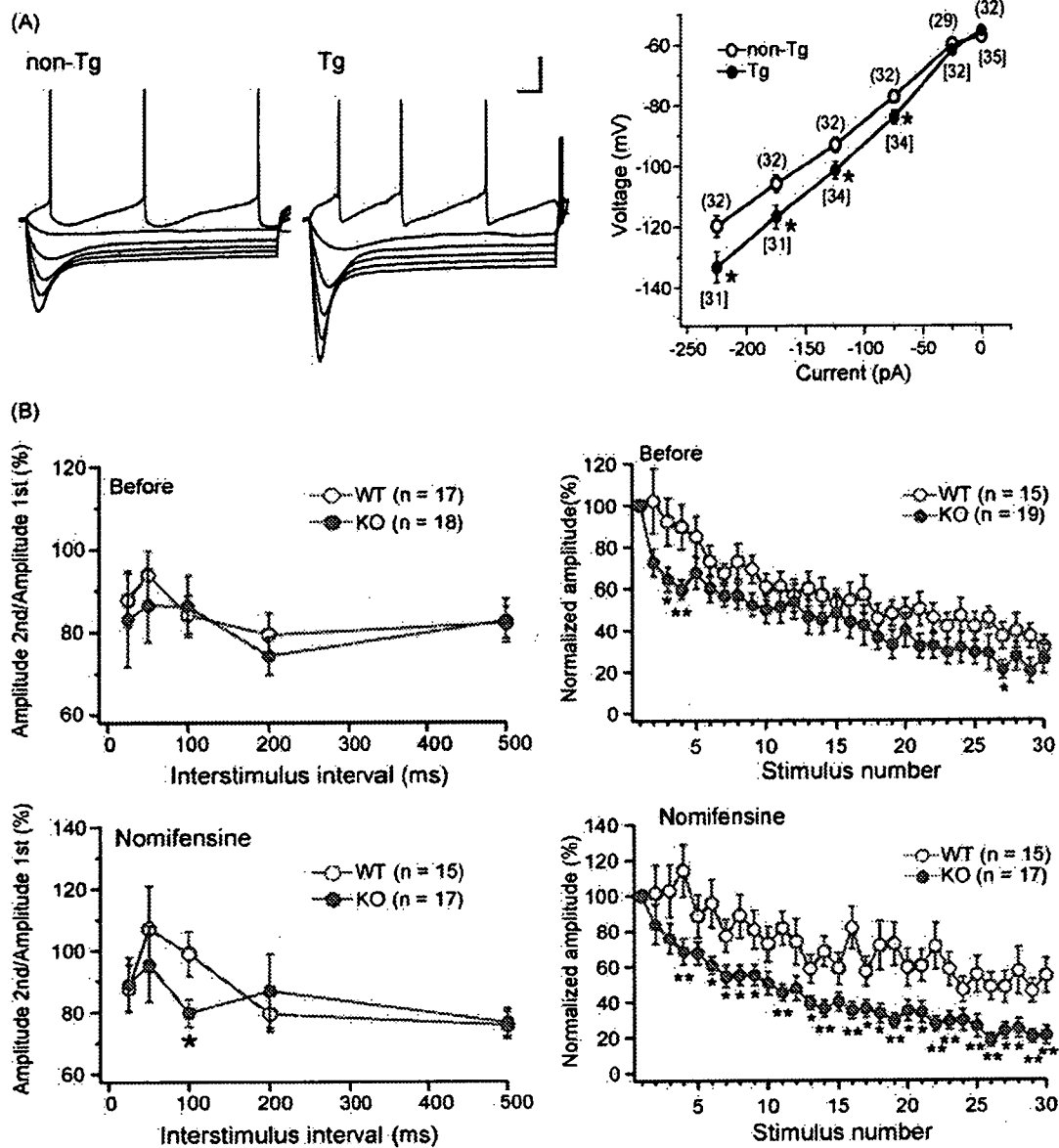
Fig. 6. Effects of Pael-R expression on physiological properties of DA neurons. (A) Sample waveforms of DA neurons taken from a non-Tg and a PrP-Tg mouse (left). Current–voltage relationships generated by injecting current pulses and recording the voltage deflections are shown on the right. Numbers in parenthesis show the numbers of cells sampled. Calibration, 25 mV, 100 ms. Input resistance in PrP-Tg mice is larger than that in non-Tg mice. *$P < 0.05$. (B) Effects of paired pulse stimulation and repeated low frequency stimulation before and after nomifensine in Pael-R KO mice. At left are shown plots of the mean (±S.E.M.) percentage of the second IPSC with respect to the first IPSC as a function of interstimulus interval before (upper) and after (lower) nomifensine application. After nomifensine treatment (3 μM), paired pulse depression (PPD) observed in wild types (WT, open circles) changed into small paired pulse facilitation (PPF), whereas PPD in knockouts (KO, gray circles) remained unchanged, yielding significant difference in paired pulse ratios at 100 ms ($P < 0.05$). Amplitudes (mean ± S.E.M.) of successive IPSCs in a burst of 30 applied 70 ms apart (i.e. at 14 Hz) normalized with respect to the amplitude of the first IPSC of the burst are shown on the right. There was a significant decrease in normalized IPSC amplitude in Pael-R KO mice (Student's t-test, $P < 0.05$) both before (upper) and after (lower) nomifensine treatment.

the change in DA content at this stage may be too small to detect nigrostriatal abnormalities in our electrophysiological analysis.

4. Discussion

Pael-R, transcripts of which are exclusively expressed in the CNS and testis, is a putative G protein coupled receptor (Donohue et al., 1998; Kawasawa et al., 2003). Unfolded Pael-R is thought to have a role in the etiology of AR-JP (Imai et al., 2001; Yang et al., 2003). Moreover, Pael-R-immunoreactivity has been observed in Lewy bodies of PD patients (Murakami

et al., 2004). These reports suggest that unfolded Pael-R is associated with degeneration of DA neurons in PD. However, the physiological function of Pael-R in the CNS remains unknown. Our investigation of Pael-R-deficient and Pael-R Tg mice here revealed its physiological function as well as its pathological function in nigrostriatal system.

Although in Pael-R-deficient mice the number of TH-positive neurons in the SN was only slightly reduced, the striatal level of DA was significantly reduced. The alteration of DA content in these mice cannot simply be explained by a change of TH (a rate-limiting enzyme of DA synthesis, converting tyrosine into

L-DOPA) or aromatic amino acid decarboxylase (AADC, the enzyme that converts L-DOPA to dopamine) expression at protein level because the change of those expressions was not observed by Western blot analysis (data not shown). We also failed to detect a significant difference in the steady state and METH-stimulated levels of DA in the striatal CSF of Pael-R KO mice or a behavioral difference following METH administration. Thus, the reduction in whole striatal DA content could come from a non-releasable pool of DA in DA neurons.

The observations of Pael-R KO mice by Marazziti et al. (2004) is almost consistent with the results of our Pael-R KO mice. However, we do not see a significant reduction in the body weights of Pael-R KO mice and a significant defect of motor performance in the rotarod test. Another difference is their mice were supersensitive to amphetamine as assessed by locomotor activity, whereas we failed to find a significant difference in the amount of METH-stimulated DA in the CSF of Pael-R KO mice. These inconsistencies may come from tested ages of the mice and a difference in genetic backgrounds (100% C57BL/6J in this study *versus* 75% C57BL/6J and 25% 129P2/OlaHsd mixed background in the previous study by Marazziti's group). We analyzed older mice (12-month-old for measurement of body weight and rotarod test, 6–12-month-old for METH administration) compared with those (2.5–4-month-old) in Marazziti's group. As a result, a compensation for Pael-R-deficiency may go on with age.

The electrophysiological analysis was done only in young mice (3–4-week-old) for technical reasons. We found that the DA neuron and striatal MSN input resistance significantly increased in PrP-Tg mice and striatal MSN input resistance significantly decreased in Pael-R KO although the resting membrane potentials, the firing thresholds, and the amplitudes and widths of the spikes remained unchanged. This observation suggests that Pael-R may interact with certain membrane factor(s) that determine the input resistance and thereby play an important role in membrane constitution. On the other hand, the finding that PPR was not altered in either Pael-R Tg or KO mice indicates that Pael-R does not affect the GABA release machinery. However, the decrement of PPR was evident after nomifensine treatment and after repeated low frequency stimulation in Pael-R KO mice compared with WT littermates. This result indicates that the absence of Pael-R depletes available striatal DA content, which might be consistent with a very recent report that the population of the cell-surface DAT at the presynapse of Pael-R KO mice is increased by the absence of direct interaction between Pael-R and DAT (Marazziti et al., 2007). Another recent study on a candidate of Pael-R ligands has showed that Pael-R is internalized upon stimulation by a neuropeptide head activator (HA) (Rezgaoui et al., 2006). Given that Pael-R is one of DAT-associated proteins, the cell-surface DAT may be internalized together with Pael-R upon HA stimulation. That could cause the extracellular accumulation of DA. However, the observations that Pael-R KO mice and Pael-R Tg mice are respectively resistant and susceptible to DA neurotoxins suggest that there are DAT-independent mechanisms of MPTP toxicity.

Growing numbers of reports have shown that increased DA levels affect terminal degeneration of DA neurons and that DA treatment leads to cell death *in vitro* (Ben-Shachar et al., 2004; Cantuti-Castelvetri et al., 2003; Hastings et al., 1996; LaVoie and Hastings, 1999; Masserano et al., 1996; Rabinovic et al., 2000; Xu et al., 2002; Zigmond et al., 2002). Moreover, although differing from classic Lewy bodies, dopamine-dependent neuronal inclusions have been experimentally generated in mice and cultured cells treated with METH (Fornai et al., 2004). The fact that various antioxidants can prevent DA neurotoxicity suggests oxidative stress occurring during DA metabolism might damage crucial neuronal functions and reduce survival. Indeed, the aging of human brain, which is an important risk factor for PD, is closely associated with attenuated antioxidant pathways challenged by oxidative stress (Lee et al., 2000; Lu et al., 2004). Considering constitutively high DA levels might expose DA neurons to chronic oxidative stress, one can assume Pael-R Tg mice are more sensitive than WT littermates to DA neurotoxins. DA neurotoxins such as MPTP and 6-OHDA are thought to disturb the mitochondrial activity of DA neurons possibly by promoting leakage of electrons from the mitochondrial electron transfer system and thereby generating reactive oxygen species. The levels of DAT and VMAT2 are reported to determine the sensitivity of neurons to DA neurotoxins. However, the resistance of Pael-R KO mice to MPTP was not explained by cell-surface levels of DAT in the striatum, which was shown to be significantly increased in Pael-R KO mice (Marazziti et al., 2007). The examination of cell-surface DAT level of Pael-R Tg mice, therefore, will be important to elucidate whether their sensitivity to DA neurotoxins is based on DAT-dependent mechanisms involving dysregulation of DA metabolism in the future.

Our results from Pael-R mutant mice strongly suggest that the Pael-R signal regulates the amount of DA in the dopaminergic neurons and that excessive Pael-R expression renders dopaminergic neurons susceptible to chronic DA toxicity. Further analysis of Pael-R mutant mice could provide useful information on the nigrostriatal DA metabolism and therapeutic strategy of PD.

Acknowledgments

References

Bamford, N.S., Zhang, H., Schmitz, Y., Wu, N.P., Cepeda, C., Levine, M.S., Schmauss, C., Zakharenko, S.S., Zablow, L., Sulzer, D., 2004. Heterosy-

naptic dopamine neurotransmission selects sets of corticostriatal terminals. Neuron 42, 653–663.

Ben-Shachar, D., Zuk, R., Gazawi, H., Ljubuncic, P., 2004. Dopamine toxicity involves mitochondrial complex I inhibition: implications to dopamine-related neuropsychiatric disorders. Biochem. Pharmacol. 67, 1965–1974.

Betarbet, R., Sherer, T.B., Greenamyre, J.T., 2002. Animal models of Parkinson's disease. Bioessays 24, 308–318.

Borchelt, D.R., Davis, J., Fischer, M., Lee, M.K., Slunt, H.H., Ratovitsky, T., Regard, J., Copeland, N.G., Jenkins, N.A., Sisodia, S.S., Price, D.L., 1996. A vector for expressing foreign genes in the brains and hearts of transgenic mice. Genet. Anal. 13, 159–163.

Calabresi, P., Fedele, E., Pisani, A., Fontana, G., Mercuri, N.B., Bernardi, G., Raiteri, M., 1995. Transmitter release associated with long-term synaptic depression in rat corticostriatal slices. Eur. J. Neurosci. 7, 1889–1894.

Cantuti-Castelvetri, I., Shukitt-Hale, B., Joseph, J.A., 2003. Dopamine neurotoxicity: age-dependent behavioral and histological effects. Neurobiol. Aging 24, 697–706.

Centonze, D., Picconi, B., Baunez, C., Borrelli, E., Pisani, A., Bernardi, G., Calabresi, P., 2002. Cocaine and amphetamine depress striatal GABAergic synaptic transmission through D2 dopamine receptors. Neuropsychopharmacology 26, 164–175.

Centonze, D., Grande, C., Usiello, A., Gubellini, P., Erbs, E., Martin, A.B., Pisani, A., Tognazzi, N., Bernardi, G., Moratalla, R., Borrelli, E., Calabresi, P., 2003. Receptor subtypes involved in the presynaptic and postsynaptic actions of dopamine on striatal interneurons. J. Neurosci. 23, 6245–6254.

Centonze, D., Gubellini, P., Usiello, A., Rossi, S., Tscherter, A., Bracci, E., Erbs, E., Tognazzi, N., Bernardi, G., Pisani, A., Calabresi, P., Borrelli, E., 2004. Differential contribution of dopamine D2S and D2L receptors in the modulation of glutamate and GABA transmission in the striatum. Neuroscience 129, 157–166.

Chui, D.H., Tanahashi, H., Ozawa, K., Ikeda, S., Checler, F., Ueda, O., Suzuki, H., Araki, W., Inoue, H., Shirotani, K., Takahashi, K., Gallyas, F., Tabira, T., 1999. Transgenic mice with Alzheimer presenilin 1 mutations show accelerated neurodegeneration without amyloid plaque formation. Nat. Med. 5, 560–564.

Donohue, P.J., Shapira, H., Mantey, S.A., Hampton, L.L., Jensen, R.T., Battey, J.F., 1998. A human gene encodes a putative G protein-coupled receptor highly expressed in the central nervous system. Brain Res. Mol. Brain Res. 54, 152–160.

Fornai, F., Lenzi, P., Gesi, M., Soldani, P., Ferrucci, M., Lazzeri, G., Capobianco, L., Battaglia, G., De Blasi, A., Nicoletti, F., Paparelli, A., 2004. Methamphetamine produces neuronal inclusions in the nigrostriatal system and in PC12 cells. J. Neurochem. 88, 114–123.

Fumagalli, F., Gainetdinov, R.R., Valenzano, K.J., Caron, M.G., 1998. Role of dopamine transporter in methamphetamine-induced neurotoxicity: evidence from mice lacking the transporter. J. Neurosci. 18, 4861–4869.

Goldberg, M.S., Fleming, S.M., Palacino, J.J., Cepeda, C., Lam, H.A., Bhatnagar, A., Meloni, E.G., Wu, N., Ackerson, L.C., Klapstein, G.J., Gajendiran, M., Roth, B.L., Chesselet, M.F., Maidment, N.T., Levine, M.S., Shen, J., 2003. Parkin-deficient mice exhibit nigrostriatal deficits but not loss of dopaminergic neurons. J. Biol. Chem. 278, 43628–43635.

Gomi, H., Yokoyama, T., Fujimoto, K., Ikeda, T., Katoh, A., Itoh, T., Itohara, S., 1995. Mice devoid of the glial fibrillary acidic protein develop normally and are susceptible to scrapie prions. Neuron 14, 29–41.

Hastings, T.G., Lewis, D.A., Zigmond, M.J., 1996. Role of oxidation in the neurotoxic effects of intrastriatal dopamine injections. Proc. Natl. Acad. Sci. U.S.A. 93, 1956–1961.

Imai, Y., Soda, M., Takahashi, R., 2000. Parkin suppresses unfolded protein stress-induced cell death through its E3 ubiquitin–protein ligase activity. J. Biol. Chem. 275, 35661–35664.

Imai, Y., Soda, M., Inoue, H., Hattori, N., Mizuno, Y., Takahashi, R., 2001. An unfolded putative transmembrane polypeptide, which can lead to endoplasmic reticulum stress, is a substrate of Parkin. Cell 105, 891–902.

Imai, Y., Soda, M., Hatakeyama, S., Akagi, T., Hashikawa, T., Nakayama, K.I., Takahashi, R., 2002. CHIP is associated with Parkin, a gene responsible for familial Parkinson's disease, and enhances its ubiquitin ligase activity. Mol. Cell. 10, 55–67.

Itier, J.M., Ibanez, P., Mena, M.A., Abbas, N., Cohen-Salmon, C., Bohme, G.A., Laville, M., Pratt, J., Corti, O., Pradier, L., Ret, G., Joubert, C., Periquet, M.,

Araujo, F., Negroni, J., Casarejos, M.J., Canals, S., Solano, R., Serrano, A., Gallego, E., Sanchez, M., Denefle, P., Benavides, J., Tremp, G., Rooney, T.A., Brice, A., Garcia de Yebenes, J., 2003. Parkin gene inactivation alters behaviour and dopamine neurotransmission in the mouse. Hum. Mol. Genet. 12, 2277–2291.

Ito, S., Kato, T., Fujita, K., 1988. Covalent binding of catechols to proteins through the sulphydryl group. Biochem. Pharmacol. 37, 1707–1710.

Kaneko, S., Hikida, T., Watanabe, D., Ichinose, H., Nagatsu, T., Kreitman, R.J., Pastan, I., Nakanishi, S., 2000. Synaptic integration mediated by striatal cholinergic interneurons in basal ganglia function. Science 289, 633–637.

Kawasawa, Y., McKenzie, L.M., Hill, D.P., Bono, H., Yanagisawa, M., 2003. G protein-coupled receptor genes in the FANTOM2 database. Genome Res. 13, 1466–1477.

Kitada, T., Asakawa, S., Hattori, N., Matsumine, H., Yamamura, Y., Minoshima, S., Yokochi, M., Mizuno, Y., Shimizu, N., 1998. Mutations in the parkin gene cause autosomal recessive juvenile parkinsonism. Nature 392, 605–608.

LaVoie, M.J., Hastings, T.G., 1999. Dopamine quinone formation and protein modification associated with the striatal neurotoxicity of methamphetamine: evidence against a role for extracellular dopamine. J. Neurosci. 19, 1484–1491.

Lee, C.K., Weindruch, R., Prolla, T.A., 2000. Gene-expression profile of the ageing brain in mice. Nat. Genet. 25, 294–297.

Lu, T., Pan, Y., Kao, S.Y., Li, C., Kohane, I., Chan, J., Yankner, B.A., 2004. Gene regulation and DNA damage in the ageing human brain. Nature 429, 883–891.

Marazziti, D., Gallo, A., Golini, E., Matteoni, R., Tocchini-Valentini, G.P., 1998. Molecular cloning and chromosomal localization of the mouse Gpr37 gene encoding an orphan G-protein-coupled peptide receptor expressed in brain and testis. Genomics 53, 315–324.

Marazziti, D., Golini, E., Mandillo, S., Magrelli, A., Witke, W., Matteoni, R., Tocchini-Valentini, G.P., 2004. Altered dopamine signaling and MPTP resistance in mice lacking the Parkinson's disease-associated GPR37/parkin-associated endothelin-like receptor. Proc. Natl. Acad. Sci. U.S.A. 101, 10189–10194.

Marazziti, D., Mandillo, S., Di Pietro, C., Golini, E., Matteoni, R., Tocchini-Valentini, G.P., 2007. GPR37 associates with the dopamine transporter to modulate dopamine uptake and behavioral responses to dopaminergic drugs. Proc. Natl. Acad. Sci. U.S.A. 104, 9846–9851.

Masserano, J.M., Gong, L., Kulaga, H., Baker, I., Wyatt, R.J., 1996. Dopamine induces apoptotic cell death of a catecholaminergic cell line derived from the central nervous system. Mol. Pharmacol. 50, 1309–1315.

Murakami, T., Shoji, M., Imai, Y., Inoue, H., Kawarabayashi, T., Matsubara, E., Harigaya, Y., Sasaki, A., Takahashi, R., Abe, K., 2004. Pael-R is accumulated in Lewy bodies of Parkinson's disease. Ann. Neurol. 55, 439–442.

Nelson, E.L., Liang, C.L., Sinton, C.M., German, D.C., 1996. Midbrain dopaminergic neurons in the mouse: computer-assisted mapping. J. Comp. Neurol. 369, 361–371.

Rabinovic, A.D., Lewis, D.A., Hastings, T.G., 2000. Role of oxidative changes in the degeneration of dopamine terminals after injection of neurotoxic levels of dopamine. Neuroscience 101, 67–76.

Rezgaoui, M., Susens, U., Ignatov, A., Gelderblom, M., Glassmeier, G., Franke, I., Urny, J., Imai, Y., Takahashi, R., Schaller, H.C., 2006. The neuropeptide head activator is a high-affinity ligand for the orphan G-protein-coupled receptor GPR37. J. Cell. Sci. 119, 542–549.

Shimura, H., Hattori, N., Kubo, S., Mizuno, Y., Asakawa, S., Minoshima, S., Shimizu, N., Iwai, K., Chiba, T., Tanaka, K., Suzuki, T., 2000. Familial Parkinson disease gene product, parkin, is a ubiquitin–protein ligase. Nat. Genet. 25, 302–305.

Sunaga, S., Maki, K., Komagata, Y., Ikuta, K., Miyazaki, J.I., 1997. Efficient removal of loxP-flanked DNA sequences in a gene-targeted locus by transient expression of Cre recombinase in fertilized eggs. Mol. Reprod. Dev. 46, 109–113.

Tateno, M., Sadakata, H., Tanaka, M., Itohara, S., Shin, R.M., Miura, M., Masuda, M., Aosaki, T., Urushitani, M., Misawa, H., Takahashi, R., 2004. Calcium-permeable AMPA receptors promote misfolding of mutant SOD1 protein and development of amyotrophic lateral sclerosis in a transgenic mouse model. Hum. Mol. Genet. 13, 2183–2196.

Valdenaire, O., Giller, T., Breu, V., Ardati, A., Schweizer, A., Richards, J.G., 1998. A new family of orphan G protein-coupled receptors predominantly expressed in the brain. FEBS Lett. 424, 193–196.

West, M.J., 1999. Stereological methods for estimating the total number of neurons and synapses: issues of precision and bias. Trends Neurosci. 22, 51–61.

Wieczorek, W.J., Kruk, Z.L., 1994. A quantitative comparison on the effects of benztropine, cocaine and nomifensine on electrically evoked dopamine overflow and rate of re-uptake in the caudate putamen and nucleus accumbens in the rat brain slice. Brain Res. 657, 42–50.

Xu, J., Kao, S.Y., Lee, F.J., Song, W., Jin, L.W., Yankner, B.A., 2002. Dopamine-dependent neurotoxicity of alpha-synuclein: a mechanism for selective neurodegeneration in Parkinson disease. Nat. Med. 8, 600–606.

Yanagawa, Y., Kobayashi, T., Ohnishi, M., Tamura, S., Tsuzuki, T., Sanbo, M., Yagi, T., Tashiro, F., Miyazaki, J., 1999. Enrichment and efficient screening of ES cells containing a targeted mutation: the use of DT-A gene with the polyadenylation signal as a negative selection maker. Transgenic Res. 8, 215–221.

Yang, Y., Nishimura, I., Imai, Y., Takahashi, R., Lu, B., 2003. Parkin suppresses dopaminergic neuron-selective neurotoxicity induced by Pael-R in *Drosophila*. Neuron 37, 911–924.

Zhang, Y., Gao, J., Chung, K.K., Huang, H., Dawson, V.L., Dawson, T.M., 2000. Parkin functions as an E2-dependent ubiquitin–protein ligase and promotes the degradation of the synaptic vesicle-associated protein, CDCrel-1. Proc. Natl. Acad. Sci. U.S.A. 97, 13354–13359.

Zhou, Q.Y., Palmiter, R.D., 1995. Dopamine-deficient mice are severely hypoactive, adipsic, and aphagic. Cell 83, 1197–1209.

Zigmond, M.J., Hastings, T.G., Perez, R.G., 2002. Increased dopamine turnover after partial loss of dopaminergic neurons: compensation or toxicity? Parkinsonism Relat. Disord. 8, 389–393.

BRIEF COMMUNICATIONS

Astrocytes as determinants of disease progression in inherited amyotrophic lateral sclerosis

Koji Yamanaka[1,2], Seung Joo Chun[1], Severine Boillee[1],
Noriko Fujimori-Tonou[2], Hirofumi Yamashita[2],
David H Gutmann[3], Ryosuke Takahashi[4], Hidemi Misawa[5] &
Don W Cleveland[1]

Dominant mutations in superoxide dismutase cause amyotrophic lateral sclerosis (ALS), an adult-onset neurodegenerative disease that is characterized by the loss of motor neurons. Using mice carrying a deletable mutant gene, diminished mutant expression in astrocytes did not affect onset, but delayed microglial activation and sharply slowed later disease progression. These findings demonstrate that mutant astrocytes are viable targets for therapies for slowing the progression of non–cell autonomous killing of motor neurons in ALS.

ALS is an adult-onset neurodegenerative disease, characterized by a progressive and fatal loss of motor neurons. Dominant mutations in the gene for superoxide dismutase (SOD1) are the most frequent cause of inherited ALS. Ubiquitous expression of mutant SOD1 in rodents leads to progressive, selective motor neuron degeneration as a result of acquired toxic properties. The exact mechanism responsible for motor neuron degeneration in ALS, however, is not known[1,2]. Mutant damage in the vulnerable motor neurons is a key determinant of disease onset[3], whereas accumulating evidence supports an active role of non-neuronal cells in motor neuron degeneration[3–7]. Evidence with selective gene excision[3] or bone-marrow grafting[5] has demonstrated that mutant SOD1-derived damage in microglia accelerates later disease progression. Despite the importance of astrocyte function, the role of mutant action in astrocytes in disease has not been tested in vivo.

To examine whether mutant SOD1 damage in astrocytes contributes to disease, loxSOD1[G37R] mice[3], carrying a mutant SOD1 gene that can be deleted by the action of the Cre recombinase, were mated with GFAP-Cre mice (Fig. 1 and Supplementary Fig. 1 online), which express both Cre recombinase and β-galactosidase (LacZ) under the control of the human GFAP promoter[8]. Mice from these matings that carry the GFAP-Cre transgene are denoted as Cre[+], whereas mice without it are referred to as Cre[-]. To determine the cell-type specificity of Cre expression in the spinal cord, GFAP-Cre mice were mated to Rosa26 mice, which ubiquitously express a LacZ gene that encodes

functional β-galactosidase only after Cre-mediated recombination. Although this GFAP-Cre transgene is expressed in a subset of neurons in the cerebellum and hippocampus during embryogenesis[9], measurement of β-galactosidase activity (by deposition of a blue reaction product after addition of the X-gal substrate) demonstrated that Cre expression and Cre-mediated recombination was restricted in the spinal cord to GFAP-reactive astrocytes (Fig. 1a,b). The efficiency of mutant gene excision in cultured astrocytes from newborn loxSOD1[G37R]/GFAP-Cre[+] mice was ~76% (Fig. 1d,e), determined by quantitative PCR for human SOD1 transgene number (Fig. 1d) and immunoblotting for mutant SOD1 levels (Fig. 1e). We observed neither detectable Cre activity nor mutant gene excision in microglia (Fig. 1c and Supplementary Fig. 2 online).

A simple, objective measure of disease onset and early disease was applied by initiation of weight loss, itself reflecting denervation-induced muscle atrophy. Reduction of SOD1[G37R] in astrocytes did not slow disease onset nor early disease (GFAP-Cre[+], 341.6 ± 48.9 d; GFAP-Cre[-], 337.0 ± 35.8 d; Fig. 1f,h). However, late disease progression (from early disease to end stage) was sharply delayed, providing a mean extension of survival by 48 d (Cre[+], 87.4 d; Cre[-], 39.5 d; Fig. 1j). Progression from onset to early disease was more modestly slowed by 14 d (Cre[+], 99.3 d; Cre[-], 85.2 d; Fig. 1i). Overall survival was extended by 60 d (Cre[+], 436.5 ± 38.8 d; Cre[-], 376.5 ± 26.9 d; Fig. 1g). This contrasts with delayed disease onset from diminished mutant synthesis solely within motor neurons (with a VAChT-Cre transgene carrying the motor neuron–specific vesicular acetylcholine transporter promoter) without affecting disease progression (Supplementary Results, Supplementary Methods and Supplementary Fig. 3 online), just as reported previously with an Isl1 (Islet1)-Cre transgene that is expressed in motor neurons and some peripheral tissues[3].

Astrocytic and microglial cell activation is a well-accepted feature of SOD1 mutant–mediated ALS[1,2]. An elevated proportion of GFAP-positive astrocytes appeared before disease onset (Fig. 2a) in loxSOD1[G37R] mice. This astrogliosis was progressive, readily apparent by onset (Fig. 2b) and more prominent during disease progression (Fig. 2c). Despite substantial mutant reduction, astrogliosis was not, however, different in comparing disease-matched loxSOD1[G37R]/GFAP-Cre[+] mice (Fig. 2d,e) and loxSOD1[G37R]/GFAP-Cre[-] mice (Fig. 2b,c).

Microglial activation occurred at earliest disease onset in Cre[-] mice (Fig. 2g) and was progressively more prominent during disease progression (Fig. 2h). Microglial activation was, however, substantially delayed from onset through early disease in the GFAP-Cre[+] mice when mutant SOD1 levels were reduced only in astrocytes (Fig. 2i,j). By exploiting the presence of β-galactosidase to mark astrocytes with diminished SOD1 mutant synthesis, examination of sections throughout lumbar spinal cords of symptomatic loxSOD1[G37R]/GFAP-Cre[+] mice

[1]Ludwig Institute for Cancer Research and Department of Medicine and Neuroscience, University of California at San Diego, 9500 Gilman Drive, La Jolla, California 92093-0670, USA. [2]Yamanaka Research Unit, RIKEN Brain Science Institute, 2-1 Hirosawa, Wako, Saitama 351-0198, Japan. [3]Department of Neurology, Washington University School of Medicine, 660 South Euclid Avenue, St. Louis, Missouri 63110, USA. [4]Department of Neurology, Graduate School of Medicine, Kyoto University, 54 Shogoin Kawahara-cho, Sakyo-ku, Kyoto 606-8507, Japan. [5]Department of Pharmacology, Kyoritsu University of Pharmacy, 1-5-30 Shibakoen, Minato-ku, Tokyo 105-8512, Japan. Correspondence should be addressed to D.W.C. (dcleveland@ucsd.edu) or K.Y. (kyamanaka@brain.riken.jp).
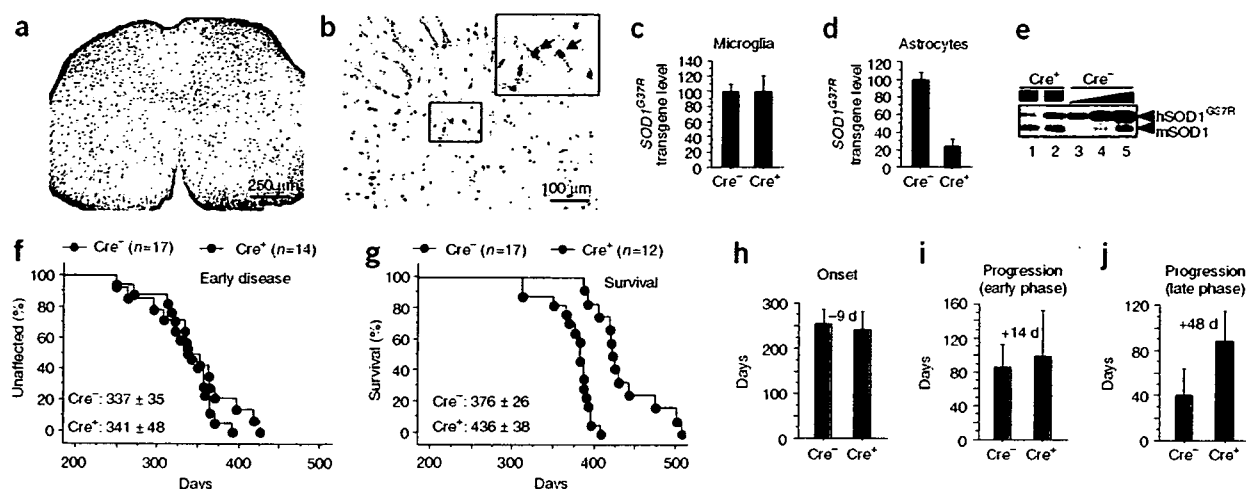
251

Figure 1 Selective Cre-mediated gene excision shows that mutant SOD1 action in astrocytes is a primary determinant of late disease progression. (a,b) β-galactosidase (β-gal) activity in astrocytes in whole (a) or in the anterior horn region (b) of the lumbar spinal cord section of GFAP-Cre/Rosa26 reporter mice visualized with X-gal and immunostaining with GFAP antibody. Inset, magnified image of the boxed area in b. Arrows indicate β-gal/GFAP-Cre-expressing astrocytes. (c,d) loxSOD1^{G37R} transgene levels (n = 3 for each group) in primary microglia (c) or astrocytes (d) from loxSOD1^{G37R}/GFAP-Cre$^+$ and loxSOD1^{G37R} mice using real-time PCR. (e) We determined SOD1^{G37R} and mouse SOD1 levels by immunoblotting extracts from isolated primary astrocytes of loxSOD1^{G37R}/GFAP-Cre$^+$ (lanes 1, 2) and a dilution series of a comparable extract from LoxSOD1^{G37R} astrocytes representing 25%, 50% and 100% of the protein amounts loaded in lanes 1 and 2 (lanes 3–5). (f,g) Ages at which early disease phase (to 10% weight loss, P = 0.76; f) or end-stage disease (P < 0.0001; g) were reached for loxSOD1^{G37R}/GFAP-Cre$^+$ mice (red) and loxSOD1^{G37R} littermates (blue). Mean ages ± s.d. are provided. (h–j) Mean onset (P = 0.47) (h), mean duration of early disease (from onset to 10% weight loss, P = 0.35; i) and a late disease (from 10% weight loss to end stage, P < 0.0001; j) for loxSOD1^{G37R}/GFAP-Cre$^+$ (red) and loxSOD1^{G37R} littermates (blue). At each time point, P value was determined by unpaired t-test. Error bars denote s.d.

revealed an inverse relationship (Fig. 3a–g) between the number of astrocytes with reduced mutant SOD1 (Cre$^+$) and activated microglia (correlation coefficient, r = −0.868, P < 0.001), despite comparable astrocytic activation. Thus, microglial activation was most prominent in areas with the highest mutant SOD1-expressing astrocyte concentration.

Elevated production of nitric oxide by upregulated inducible nitric oxide synthase (iNOS) has been reported in mutant SOD1 mice[10], although deletion of the iNOS gene has modest[11] or no[12] effect on SOD1-mediated disease. It is not known in which glial cells this nitric oxide is produced in in vivo models of ALS, although both microglia and astrocytes have an ability to produce it when stimulated in vitro[13]. Triple staining of lumbar spinal cord sections with iNOS, Mac2 and GFAP antibodies (Fig. 3h–r) revealed that almost all iNOS-positive cells were

Mac2-positive microglia (Fig. 3n–r and Supplementary Fig. 4 online), indicating that activated microglia are the primary cell type producing nitric oxide in this SOD1 mouse model. Diminishing mutant synthesis in astrocytes inhibited iNOS induction in disease-matched, symptomatic SOD1 mice (Fig. 3h,k), consistent with substantial inhibition of microglial activation (Fig. 3i,l).

Figure 2 Selective downregulation of mutant SOD1 in astrocytes significantly inhibits microglial activation. (a–t) GFAP-positive astrocytes (a–e), Mac2-positive activated microglia (f–j) and motor neurons identified with the neurofilament antibody SMI-32 (k–o) in the lumbar spinal cord of a loxSOD1^{G37R} mouse before disease onset (a,f,k,p), at disease onset (b,g,l,q) or during early disease (c,h,m,r), together with loxSOD1^{G37R}/GFAP-Cre$^+$ mice at disease onset (d,i,n,s) or during early disease (e,j,o,t). Merged images are shown in p–t.
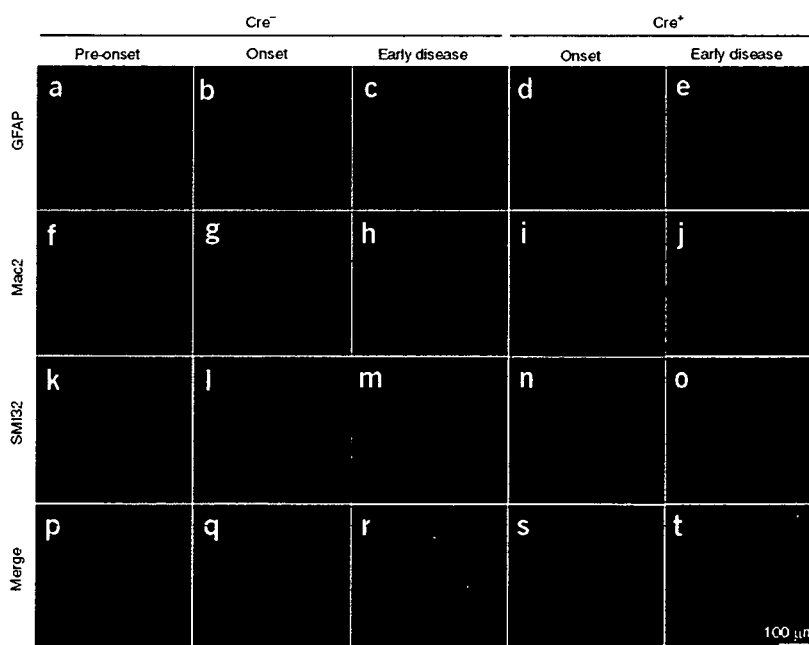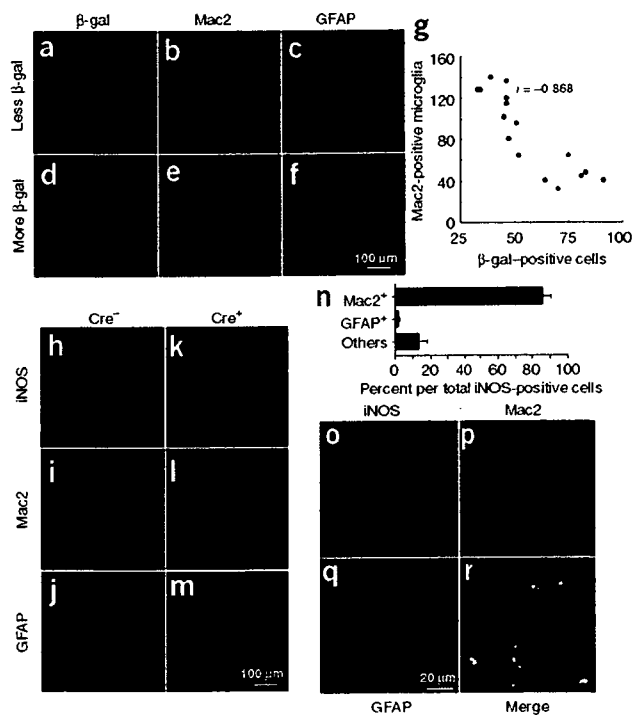
Figure 3 Mutant-expressing astrocytes enhance microglial activation and induction of iNOS. (a–f) Images of β-galactosidase (a,d), Mac2 (b,e) and GFAP (c,f) staining from a left (a–c) and right (d–f) lumbar spinal cord section from a 12-month-old loxSOD1^{G37R}/GFAP-Cre$^+$ mouse. GFAP-Cre$^+$ astrocytes are marked by β-galactosidase (a,d). (g) Inverted correlation between the number of Cre-positive astrocytes and Mac2-positive microglia in loxSOD1^{G37R}/GFAP-Cre$^+$ mice lumbar spinal cord sections (correlation coefficient, $r = -0.868$, $P < 0.001$). (h–m) Lumbar spinal cord sections from loxSOD1^{G37R} (h–j) and loxSOD1^{G37R}/GFAP-Cre$^+$ (k–m) mice at the early disease stage immunostained with antibodies to iNOS (h,k), Mac2 (i,l), and GFAP (j,m). (n) Quantification of iNOS-positive cells in the anterior horn from lumbar spinal cord of symptomatic loxSOD1^{G37R} mice. We plotted the averaged percent of iNOS$^+$/Mac2$^+$ (red), iNOS$^+$/GFAP$^+$ (blue) and iNOS$^+$/other cell type (black) per total iNOS$^+$ cells. (o–r) Magnified images of anterior horn from lumbar spinal cord of symptomatic loxSOD1^{G37R} mice stained with iNOS (o), Mac2 (p) and GFAP (q). Merged image illustrates that iNOS-positive cells are Mac2-positive microglia (r).

in ALS by supplementing healthy astrocytes or modulating toxicity in astrocytes to control an inflammatory response of microglia.

Note: Supplementary information is available on the Nature Neuroscience website.

AUTHOR CONTRIBUTIONS

K.Y., S.J.C., S.B., N.F.-T. and H.Y. conducted the experiments. D.H.G., R.T. and H.M. provided essential experimental tools and advice. K.Y., S.B., and D.W.C. were responsible for the overall design of the project, analyses of the results and writing the manuscript.

A role for astrocytes in inherited ALS has been previously considered in several contexts. Mutant-expressing astrocytes produce and release one or more as yet uncharacterized components that can accelerate motor neuron death *in vitro*[6,7]. Focal loss of the astrocytic EAAT2 glutamate transporter in affected regions[14] (Supplementary Fig. 5 online) and the failure of normal glutamate uptake of SOD1^{G93A} astrocytes *in vitro*[15] support glutamate-dependent excitotoxicity as a component of disease. Nevertheless, diminished mutant SOD1 synthesis in most astrocytes did not affect disease-dependent loss of EAAT2 from those astrocytes (Supplementary Fig. 5), indicating that a reduction in glutamate transport reflects non–cell autonomous damage to astrocytes, in part, from mutant SOD1 synthesized by other cells. Our use of selective gene excision has now demonstrated that mutant SOD1 damage in both microglia[3] and astrocytes (Fig. 1g–j) accelerates later disease progression without affecting the initiation of motor neuron degeneration and phenotypic disease onset. Discovery that damage in astrocytes determines the timing of microglial activation and infiltration provides further evidence that, beyond any direct effect of mutant astrocytes on motor neurons, such astrocytes amplify an inflammatory response from microglia (including enhanced production of nitric oxide and possibly of toxic cytokines), leading to further damage to the motor neurons and accelerated disease progression through a non–cell autonomous mechanism (Supplementary Fig. 6 online). These findings validate therapies, including astrocytic stem cell–replacement approaches, that aim to slow disease progression

1. Pasinelli, P. & Brown, R.H. *Nat. Rev. Neurosci.* **7**, 710–723 (2006).
2. Boillee, S., Vande Velde, C. & Cleveland, D.W. *Neuron* **52**, 39–59 (2006).
3. Boillee, S. *et al. Science* **312**, 1389–1392 (2006).
4. Clement, A.M. *et al. Science* **302**, 113–117 (2003).
5. Beers, D.R. *et al. Proc. Natl. Acad. Sci. USA* **103**, 16021–16026 (2006).
6. Di Giorgio, F.P., Carrasco, M.A., Siao, M.C., Maniatis, T. & Eggan, K. *Nat. Neurosci.* **10**, 608–614 (2007).
7. Nagai, M. *et al. Nat. Neurosci.* **10**, 615–622 (2007).
8. Bajenaru, M.L. *et al. Mol. Cell. Biol.* **22**, 5100–5113 (2002).
9. Fraser, M.M. *et al. Cancer Res.* **64**, 7773–7779 (2004).
10. Almer, G., Vukosavic, S., Romero, N. & Przedborski, S. *J. Neurochem.* **72**, 2415–2425 (1999).
11. Martin, L.J. *et al. J. Comp. Neurol.* **500**, 20–46 (2007).
12. Son, M., Fathallah-Shaykh, H.M. & Elliott, J.L. *Ann. Neurol.* **50**, 273 (2001).
13. Barbeito, L.H. *et al. Brain Res. Brain Res. Rev.* **47**, 263–274 (2004).
14. Howland, D.S. *et al. Proc. Natl. Acad. Sci. USA* **99**, 1604–1609 (2002).
15. Vermeiren, C. *et al. J. Neurochem.* **96**, 719–731 (2006).

ELSEVIER

Phospholipids modulate superoxide and nitric oxide production by lipopolysaccharide and phorbol 12-myristate-13-acetate-activated microglia

Sadayuki Hashioka [a,*], Youn-Hee Han [b,1], Shunsuke Fujii [c,2], Takahiro Kato [a], Akira Monji [a,**], Hideo Utsumi [b], Makoto Sawada [d], Hiroshi Nakanishi [c], Shigenobu Kanba [a]

[a] *Department of Neuropsychiatry, Graduate School of Medicine, Kyushu University, Maidashi 3-1-1, Higashi-ku, Fukuoka 812-8582, Japan*
[b] *Department of Chemo-Pharmaceutical Sciences, Graduate School of Pharmaceutical Sciences, Kyushu University, Japan*
[c] *Laboratory of Oral Aging Science, Faculty of Dental Sciences, Kyushu University, Japan*
[d] *Department of Brain Life Science, Research Institute of Environmental Medicine, Nagoya University, Japan*

Abstract

Microglial activation and inflammatory processes have been implicated in the pathogenesis of a number of neurodegenerative disorders. Recently, peroxynitrite ($ONOO^-$), the reaction product of superoxide ($^\bullet O_2^-$) and nitric oxide (NO) both of which can be generated by activated microglia, has been demonstrated to act as a major mediator in the neurotoxicity induced by activated microglia. On the other hand, phospholipids such as phosphatidylserine (PS) and phosphatidylcholine (PC) have been reported to modulate the immune function of phagocytes. We therefore evaluated the effects of liposomes which comprise both PS and PC (PS/PC liposomes) or PC only (PC liposomes) regarding the production of both $^\bullet O_2^-$ and NO by lipopolysaccharide (LPS)/phorbol 12-myristate-13-acetate (PMA)-activated microglia using electron spin resonance (ESR) spin trap technique with a DEPMPO and Griess reaction, respectively. Pretreatment with PS/PC liposomes or PC liposomes considerably inhibited the signal intensity of $^\bullet O_2^-$ adduct associated with LPS/PMA-activated microglia in a dose-dependent manner. In addition, pretreatment with PS/PC liposomes also significantly reduced LPS/PMA-induced microglial NO production. In contrast, pretreatment with PC liposomes had no effect on the NO production. These results indicate that PS/PC liposomes can inhibit the microglial production of both NO and $^\bullet O_2^-$, and thus presumably prevent a subsequent formation of $ONOO^-$. Therefore, PS/PC liposomes appear to have both neuroprotective and anti-oxidative properties through the inhibition of microglial activation.
© 2006 Elsevier Ltd. All rights reserved.

Keywords: Microglia; Superoxide; Nitric oxide; Peroxynitrite; Electron spin resonance; Phosphatidylserine; Phosphatidylcholine

1. Introduction

Increasing evidence shows that microglial activation and inflammatory processes are involved in the pathogenesis of a

* Corresponding author. Present address: Kinsmen Laboratory of Neurological Research, Department of Psychiatry, Faculty of Medicine, University of British Columbia, 2255 Wesbrook Mall, Vancouver, BC V6T 1W5, Canada. Tel.: +1 604 822 7377; fax: +1 604 822 7086.
** Corresponding author. Tel.: +81 92 642 5627; fax: +81 92 642 5644.
   E-mail addresses: hashioka@interchange.ubc.ca, hashioka@f2.dion.ne.jp (S. Hashioka), amonji@hf.rim.or.jp (A. Monji).
[1] Present address: Department of Civil and Environmental Engineering, Tohoku Gakuin University, Japan.
[2] Present address: Central Pharmaceutical Research Institute, JT Inc., Japan.

number of neurodegenerative disorders such as Alzheimer's disease (AD), Parkinson's disease (PD), amyotrophic lateral sclerosis and multiple sclerosis (MS) (McGeer et al., 1988; McGeer and McGeer, 2002; Navikas and Link, 1996). In addition, many *in vitro* studies have shown that activated microglia produce an excess of inflammatory and potentially neurotoxic molecules such as pro-inflammatory cytokines including tumor necrosis factor-α (TNF-α) and interleukin 1-β, reactive oxygen species (ROS) and reactive nitrogen species, i.e., superoxide anion ($^\bullet O_2^-$) and nitric oxide (NO) and consequently cause neuronal injury or death (Combs et al., 2001; Hashioka et al., 2005; Meda et al., 1995; Qin et al., 2002; Suuronen et al., 2006; Szelenyi et al., 2006). However, the question as to precisely which toxic agent(s) released from

activated microglia are responsible for neurotoxicity remains unclear.

Recently, peroxynitrite ($ONOO^-$), the reaction product of $^\bullet O_2^-$ and NO, has been demonstrated to act as a major mediator in the neurotoxicity induced by amyloid β (Aβ)-activated microglia in vitro (Xie et al., 2002). $ONOO^-$ is a highly reactive oxidant capable of inducing injury to a number of cell types (Torreilles et al., 1999). In support of this, $ONOO^-$ generated by lipopolysaccharide (LPS)-activated microglia has been shown to act as a primary cytotoxic factor for oligodendrocytes as well (Li et al., 2005). Therefore, the inhibition of microglial production of both NO and $^\bullet O_2^-$ and the subsequent formation of $ONOO^-$ appears to be neuroprotective and a potentially useful treatment for some kinds of neurodegenerative disorder and white matter disorder. $^\bullet O_2^-$ is not only a tally of NO for $ONOO^-$ formation but also a limiting factor for $ONOO^-$ formation (Navarro-Antolin et al., 2002; Possel et al., 2002). Furthermore, $^\bullet O_2^-$ is a precursor of the other ROS such as hydrogen peroxide (H_2O_2) and hydroxyl radical ($^\bullet OH$), and ROS has been reported to mediate pro-inflammatory signaling in activated microglia and thus amplify TNF-α production (Qin et al., 2004). It is, therefore, very important to measure microglial $^\bullet O_2^-$ production specifically and directly. Several studies using indirect methods such as cytochrome c reduction assay, nitroblue tetrazolium reduction assay and chemiluminescence assay have suggested that activated microglia posses the capacity for $^\bullet O_2^-$ production (Colton et al., 1994; Tanaka et al., 1994; Herrera-Molina and von Bernhardi, 2005). So far, however, few studies have directly identified the microglial generation of ROS including $^\bullet O_2^-$ using electron spin resonance (ESR) with the spin trap technique (Sankarapandi et al., 1998; Chang et al., 2000). Especially, to our knowledge, there has only been one study, which successfully detected the $^\bullet O_2^-$-specific spin adduct formed by activated microglia employing a 5-(diethoxyphosphoryl)-5-methyl-1-pyroline-N-oxide (DEPMPO), an apt spin trapping agent for cell-generated $^\bullet O_2^-$ (Sankarapandi et al., 1998; Shi et al., 2005).

Phospholipids such as phosphatidylserine (PS) and phosphatidylcholine (PC) have been reported to be able to modulate the immune functions of phagocytes. PC, a major component of the outer leaflet of the plasma membrane, has been demonstrated to reduce the production of ROS and TNF-α in LPS/ phorbol 12-myristate-13-acetate (PMA)-activated monocytes (Morris et al., 2000; Tonks et al., 2005). On the other hand, abnormal exposure of PS, which is normally sequestered in the inner leaflet of plasma membrane, in the early phase of apoptosis is an essential determinant for the recognition and ingestion of apoptotic cells by phagocytes (Fadok et al., 1992). After the engulfment of apoptotic cells, macrophages are well known to actively suppress the inflammatory response by releasing anti-inflammatory mediators and thus decreasing the secretion of various pro-inflammatory cytokines (Fadok et al., 1998). Furthermore, PS-containing liposomes have been shown to mimic the effects of apoptotic cells on macrophages (Fadok et al., 2000) and microglia (De Simone et al., 2002; Zhang et al., 2005) through surface molecules that recognize PS.

For the above-mentioned reasons, we evaluated the effects of liposomes comprising both PS and PC (PS/PC liposomes) or PC alone (PC liposomes) on $^\bullet O_2^-$ and NO production by LPS/ PMA-activated microglia using the ESR spin trap technique with the DEPMPO and Griess reaction, respectively. We herein provide evidence that PS/PC liposomes can inhibit the microglial production of both NO and $^\bullet O_2^-$, and thus presumably prevent the subsequent formation of $ONOO^-$.

2. Materials and methods

2.1. Chemicals and reagents

PMA was purchased from Biomol international (Plymouth Meeting, PA, USA). LPS, diethylenetriamine pentaacetic acid (DTPA), and a spintrap DEPMPO were purchased from Sigma Chemicals (St. Louis, MO, USA). Superoxide dismutase (SOD; from bovine erythrocytes, 35,000 U/mg), catalase (from beef liver, 11,500 U/mg), xanthine, and xanthine oxidase were purchased from Wako Pure Chemical Industries (Osaka, Japan). The final concentrations of SOD and catalase correspond to the enzyme activities per volume described in a previous report (Chang et al., 2000). Recombinant mouse granulocyte macrophage colony stimulating factor (GM-CSF) was purchased from R&D systems (Minneapolis, MN, USA). Porcine brain derived-L-α-PS, egg derived-L-α-PC, 4-nitrobenz-2-oxa-1,3-diazole (NBD)-labeled PS, and NBD-labeled PC were purchased from Avanti Polar Lipids (Alabaster, AL, USA).

2.2. Preparation of liposomes

The liposomes were prepared as previously described (Nishikawa et al., 1990). In brief, a mixture of 12 mM PS and 33 mM PC in chloroform was placed in a test tube. The liposomes were composed of either PC only (PC liposomes) or a combination of PS and PC at a molar ratio of 3:7 (PS/PC liposomes). The solvent was removed in a rotary evaporator at 30 °C under reduced pressure and then dried by a desiccator for 1 h. The desiccated lipids were dispersed with a vortex mixer in phosphate buffered saline (PBS) (pH 7.4) to obtain final concentrations of 10 mM total lipids. The lipid suspensions were subsequently sonicated (Tomy UR-20P, Tokyo, Japan) for 10 min on ice. The liposome solutions were centrifuged and then the supernatants were used for the assays. Using either NBD-labeled PS or NBD-labeled PC, NBD-labeled PS/PC liposomes and NBD-labeled PC liposomes were prepared by the same methods as described above.

2.3. Microglial cell cultures

The murine microglial cell line, 6-3, was established from neonatal C57BL/ 6J(H-2b) mice using a non-enzymatic and non-virus-transformed procedure (Kanzawa et al., 2000). The 6-3 cells closely resemble primary cultured microglia (Kanzawa et al., 2000; Okada et al., 2003). The 6-3 cells were cultured in Eagle's minimal essential medium, 0.3% NaHCO3, 2 mM glutamine, 0.2% glucose, 10 μg/ml insulin and 10% fetal calf serum, and maintained at 37 °C with 10% CO2, 90% air atmosphere. One nanogram per milliliter of mouse recombinant GM-CSF was supplemented in the culture medium to maintain the 6-3 cells because these cells stop to proliferate without it (Kanzawa et al., 2000). The culture media were renewed twice per week.

The primary microglial cells were isolated from mixed cell cultures from the cerebral cortex of 3-day-old Wister rats according to the methods described previously (Hashioka et al., 2005). The medium and culture conditions to maintain the primary microglia were the same as that for 6-3 cells. The culture media were renewed twice per week.

2.4. Fluorescence microscopy

After 3 h treatment of NBD-labeled PS/PC liposomes (100 μM) or NBD-labeled PC liposomes (100 μM), primary cultured rat microglia were mounted

on coverslips at a density of 1.0×10^4 cells/ml and were fixed with 4% paraformaldehyde for 30 min at room temperature. Afterwards, the images were taken at an excitation of 470 nm and an emission of 530 nm by using a fluorescence microscopy (Leica Microsystems DMRB, Wetzlar, Germany).

2.5. ESR spectroscopy

ESR, together with the spin-trapping agent DEPMPO was employed to accurately detect the production of $^{\bullet}O_2^{-}$ radicals by activated microglia. The 6-3 microglial cells were plated on 12-well tissue culture plates at a density of 1.6×10^6 cells in 400 μl of serum free culture medium per well. The 6-3 cells were incubated 500 ng/ml LPS for 16 h in the presence or absence of pretreatment of PS/PC liposomes or PC liposomes for 1 h at 37 °C. Afterwards, the 6-3 cells were incubated at 37 °C with or without 400 ng/ml PMA for 30 min before beginning the detection of ESR spectra. Cell suspensions (4×10^6 cells/ml) in the culture medium containing 25 mM DEPMPO were transferred to a standard cell capillary, and the ESR measurements were performed at room temperature right after the incubation. The ESR spectra were obtained using a JES-RE1X ESR spectrometer (JEOL, Japan). The setting conditions of the instrument were as follows: magnetic field = 336.7 ± 7.5 mT, modulation amplitude = 2000, modulation width = 0.1 mT, modulation frequency = 100 kHz, time constant = 0.1 s, microwave power = 10 mW, microwave frequency = 9430 MHz and sweep time = 2 min.

2.6. Spin trapping in xanthine/xanthine oxidase sysytem

Xanthine oxidase (0.1 U/ml) was incubated with 0.4 mM xanthine in phosphate–buffer (PB) containing 2 mM DTPA and 20 mM DEPMPO in the presence or absence of 2 mM PS/PC liposomes or PC liposomes. Xanthine oxidase was added last to the mixture to start the reaction. The ESR spectra were recorded at room temperature on a JES-RE1X ESR spectrometer. The setting conditions of the instrument were as follows: magnetic field = 336.7 ± 7.5 mT, modulation amplitude = 500, modulation width = 0.1 mT, modulation frequency = 100 kHz, time constant = 0.03 s, microwave power = 10 mW, microwave frequency = 9430 MHz and sweep time = 1 min.

2.7. NO quantification

The accumulation of NO_2^{-}, a stable end-product, extensively used as an indicator of NO production by cultured cells, was assayed by the Griess reaction. The 6-3 microglial cells were plated on 24-well tissue culture plates at 9×10^5 per 200 μl per well and incubated in the presence or absence of pretreatment of PS/PC liposomes or PC liposomes for 1 h at 37 °C. Afterwards, the cells were incubated in the presence or absence of 500 ng/ml LPS and 400 ng/ml PMA at 37 °C. After 48 h, the cell-free supernatants were mixed with equal amounts of Griess reagent (Griess Reagent Kit; Dojindo, Kumamoto, Japan). Samples were incubated at room temperature for 15 min and subsequently absorbance was read at 540 nm using a plate reader (Multiskan MS; Labsystems, UK).

2.8. Statistics

The values were expressed as the means ± S.E.M. and analyzed by a one-way analysis of variance (ANOVA) followed by Scheffe's post hoc test. The significance was established at a level of $p < 0.05$.

3. Results

3.1. Confirmation of microglial phagocytosis of PS/PC liposomes

First, in order to confirm that the PS/PC liposomes are certainly engulfed by microglia, we treated primary cultured rat microglia with NBD-labeled PS/PC liposomes or NBD-labeled PC liposomes. After 3 h of treatment, microglia were fixed with
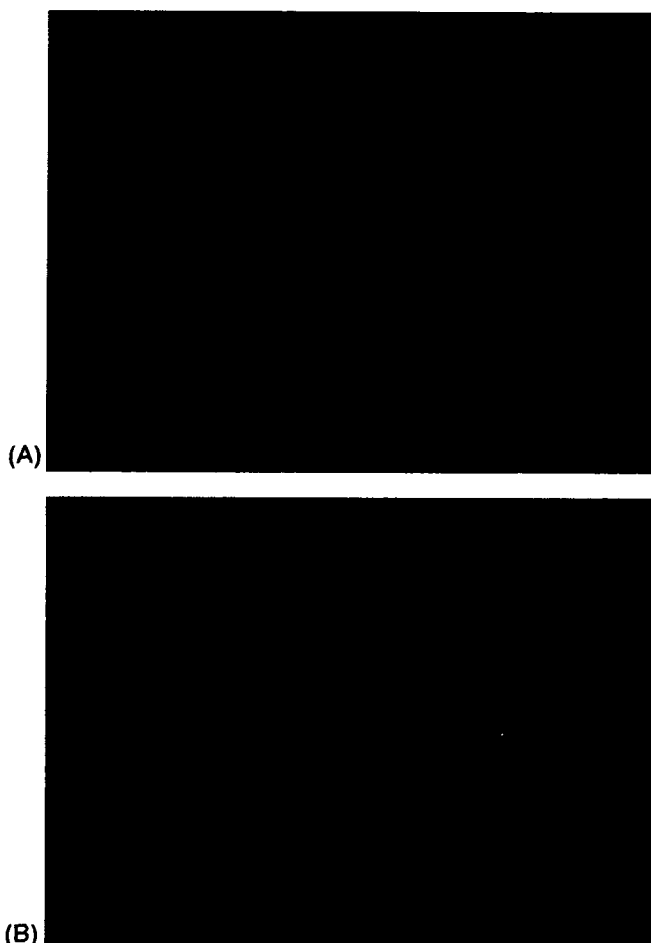

Fig. 1. Microglial phagocytosis of PS/PC liposomes. A typical fluorescence microphotograph showing (A) phagocytosis of NBD-labeled PS/PC liposomes (green) by primary cultured rat microglia and (B) little phagocytosis of NBD-labeled PC liposomes by primary cultured rat microglia.

4% PFA and examined by fluorescence microscopy. The florescent images were merged with the corresponding phase contrast images. As shown in Fig. 1A, it was observed that well-defined microglial cytoplasm was filled with florescently labeled PS/PC liposomes (green). In contrast, few PC liposomes labeled with the florescence were observed in microglial cytoplasm (Fig. 1B). These findings indicate that PS/PC liposomes, but not PC liposomes, were phagocytosed by microglia.

3.2. Effect of the liposomes on the $^{\bullet}O_2^{-}$ production by LPS/PMA-activated microglia

We subsequently measured the generation of $^{\bullet}O_2^{-}$ associated with activated microglia by ESR monitoring with a spin trap DEPMPO. In the preparations of non-stimulated microglia (Fig. 2A) and 500 ng/ml LPS alone-stimulated microglia (Fig. 2B), no signals were obtained. Microglial cells stimulated by 500 ng/ml LPS combined with 400 ng/ml PMA in the presence of 25 mM DEPMPO showed the prominent signals whose spectrum consisting of a linear combination of a characteristic 12-line spectrum corresponding to $^{\bullet}O_2^{-}$ spin
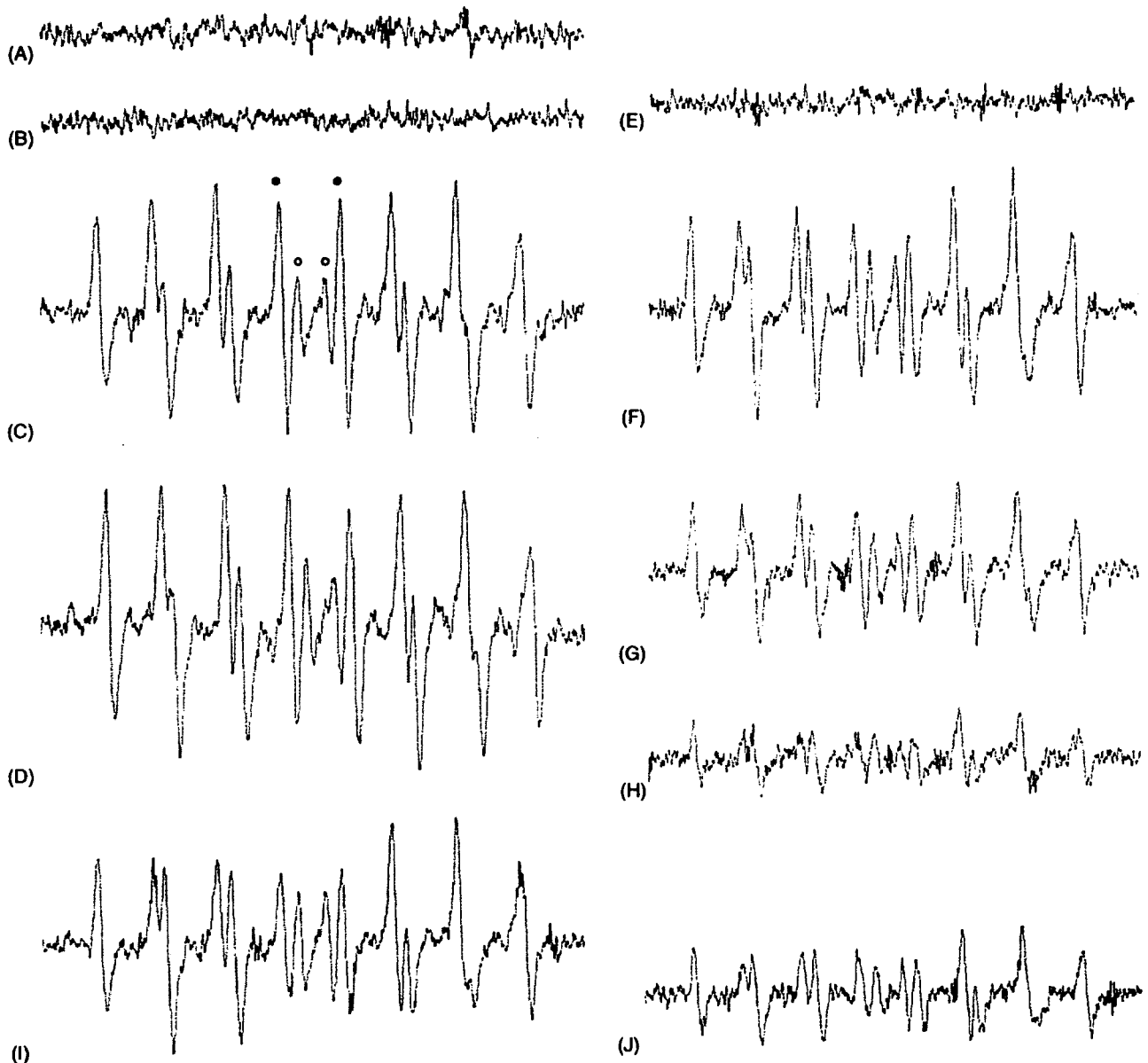
(A)

(B)

(C)

(D)

(I)

(E)

(F)

(G)

(H)

(J)

Fig. 2. Detection of $^\bullet O_2^-$ generation by LPS/PMA-activated microglia using ESR spin trap technique with DEPMPO. 6-3 microglial cells (4 × 10⁶/ml) were incubated with LPS (500 ng/ml) for 16 h and PMA (400ng/ml) for 30 min at 37 °C with or without pretreatment of PS/PC liposomes for 1 h. The ESR spectra were then recorded in the presence of 25 mM DEPMPO at room temperature. (A) ESR spectra of DEPMPO adducts obtained from non-stimulated microglia. (B) ESR spectra of DEPMPO adducts obtained from microglia stimulated by LPS (500 ng/ml) alone. (C) ESR spectra of DEPMPO adducts obtained from LPS/PMA-activated microglia. Open and closed circles represent measured signal peaks of DEPMPO–OH and DEPMPO–OOH adducts, respectively. (D) ESR spectra of DEPMPO adducts obtained from microglia stimulated by PMA (400 ng/ml) alone. (E) the same as (C), but with the addition of SOD (160 μg/ml). (F) the same as (C), but with the addition of catalase (280 μg/ml). (G) the same as (C), but after pretreatment with PS/PC liposomes (0.1 mM) for 1 h. (H) the same as (C), but after pretreatment with PS/PC liposomes (1 mM) for 1 h. (I) the same as (C), but after pretreatment with PC liposomes (0.1 mM) for 1 h. (J) the same as (C), but after pretreatment with PC liposomes (1 mM) for 1 h.

adduct DEPMPO–OOH and an eight-line spectrum corresponding to $^\bullet OH$ spin adduct DEPMPO–OH (Fig. 2C). Computer simulation confirmed DEPMPO–OOH with hyperfine splittings $a_N = 13.15$ G, $a_H^\beta = 10.59$ G, $a_p = 49.73$ G, $a_H^\gamma = 0.72$ G and DEPMPO–OH with hyperfine splittings $a_N = 12.43$ G, $a_H = 13.49$ G, $a_p = 50.39$ G. These values are consistent with those described in a previous report (Sankarapandi et al., 1998). In addition, microglial cells stimulated by 400 ng/ml PMA alone showed essentially the same ESR spectra as those of LPS/PMA-activated microglia (Fig. 2D). To further

confirm the original species of the spin adduct generated by LPS/PMA-activated microglia, SOD (160 μg/ml) or catalase (280 μg/ml) were also treated. The ESR signal intensity was substantially decreased by SOD (Fig. 2E), not by catalase (Fig. 2F). These results indicate that the spin adducts originated from $^\bullet O_2^-$ radical but not $^\bullet OH$ radical, which is derived from H_2O_2.

We next evaluated the effect of the liposomes on the generation of $^\bullet O_2^-$ associated with LPS/PMA-activated microglia. Pretreatment with PS/PC liposomes for 1 h considerably
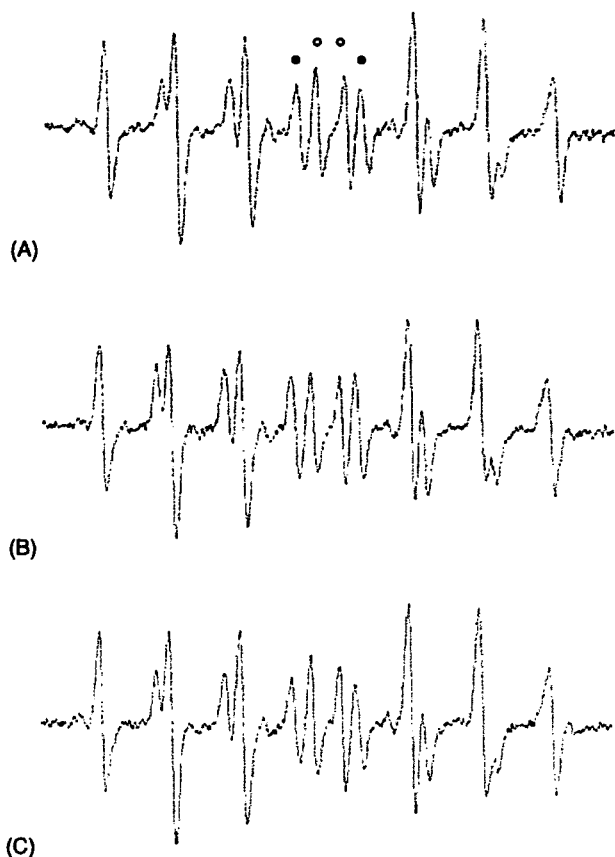
(A)

(B)

(C)

Fig. 3. Detection of $\bullet O_2^-$ generation in xanthine/xanthine oxidase system using ESR spin trap technique with DEPMPO. The system contained 0.4 mM xanthine, 2 mM DTPA, and 20 mM DEPMPO in PB in the presence or absence of 2 mM PS/PC liposomes or PC liposomes. Xanthine oxidase (0.1 U/ml) was added last to the mixture to start the reaction. (A) ESR spectra of DEPMPO adducts obtained in the xanthine/xanthine oxidase system. Open and closed circles represent measured signal peaks of DEPMPO–OH and DEPMPO–OOH adducts, respectively. (B) the same as (A), but in the presence of 2 mM PS/PC liposomes. (C) the same as (A), but in the presence of 2 mM PC liposomes.

inhibited the signal intensity of the $\bullet O_2^-$ adduct in a dose-dependent manner (Fig. 2G, H). In spite of few PC liposomes were phagocytosed by microglia, pretreatment with PC liposomes for 1 h also inhibited the signal intensity of the $\bullet O_2^-$ adduct in a dose-dependent manner (Fig. 2I, J).

3.3. Effect of the liposomes on the $\bullet O_2^-$ generation in xanthine/xanthine oxidase system

To confirm whether or not the liposomes per se scavenge $\bullet O_2^-$, we measured the $\bullet O_2^-$ production in xanthine/xanthine oxidase system in the presence or absence of the liposomes by ESR monitoring with a spin trap DEPMPO. Fig. 3A shows typical ESR spectra consisting of DEPMPO–OOH and DEPMPO–OH in xanthine/xanthine oxidase system. The formation of these spin adducts via trapping $\bullet O_2^-$ was confirmed by experiments in which SOD (160 µg/ml) was added before xanthine oxidase and ESR signals were completely quenched (data not shown), while catalase
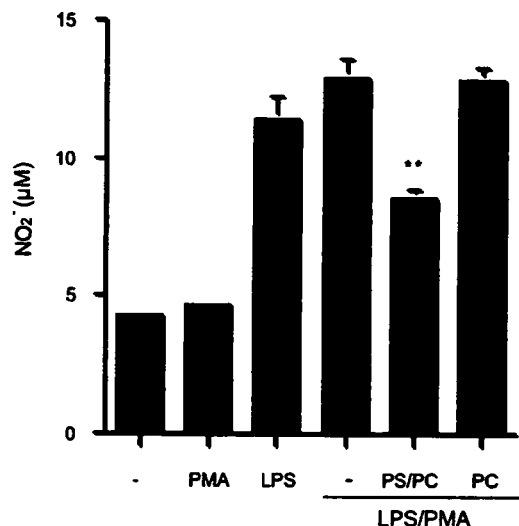

Fig. 4. Effect of the liposomes on the NO production by LPS/PMA-activated microglia. 6-3 microglial cells were incubated with LPS (500 ng/ml) and PMA (400 ng/ml) at 37 °C with or without pretreatment with 1 mM PS/PC liposomes or PC liposomes for 1 h. After 48 h, collected media were assayed for NO accumulation using the Griess reaction. $\overset{**}{p} < 0.01$, compared with LPS/PMA. The data are the mean values ± S.E.M. ($n = 3$).

(280 µg/ml) was added, in which ESR signals were not quenched at all (data not shown). The ESR spectra in the presence of either 2 mM PS/PC liposomes or PC liposomes showed essentially the same as those shown in Fig. 3A, thus indicating that neither PS/PC liposomes nor PC liposmes have scavenging effect on $\bullet O_2^-$, but have the inhibitory effect on the $\bullet O_2^-$-generating system in microglia (Fig. 3B, C).

3.4. Effect of the liposomes on the NO production by LPS/PMA-activated microglia

Using a Griess reaction assay, we investigated the effect of the liposomes on the microglial production of NO, a tally of $\bullet O_2^-$ for forming ONOO$^-$. The incubation of microglial cells with 500 ng/ml LPS combined with 400 ng/ml PMA for 48 h resulted in a significant elevation in the accumulation of nitrite (Fig. 4). Five hundred nanograms per milliliters LPS alone, also, showed nearly the same amount of microglial production of NO, whereas, 400 ng/ml PMA alone could not induce a significant increase of the NO production. As expected, the LPS/PMA-induced microglial NO production significantly decreased after pretreatment with 1 mM PS/PC liposomes for 1 h (Fig. 4). In contrast, pretreatment with 1 mM PC liposomes for 1 h did not affect the microglial NO production at all (Fig. 4).

4. Discussion

In the present study, PS/PC liposomes considerably inhibited both $\bullet O_2^-$ and NO production in LPS/PMA-activated microglia and thus presumably prevent the subsequent formation of ONOO$^-$, a powerful oxidant capable of inducing strong toxicity. ONOO$^-$ is formed from non-enzymatic reaction between $\bullet O_2^-$ and NO at the near diffusion-limited

rate whose constant is three times faster than rate at which superoxide dismutase scavenges $^{\bullet}O_2^-$ (Beckman, 1994; Torreilles et al., 1999). ONOO$^-$, therefore, can be generated in several regions *in vivo* where $^{\bullet}O_2^-$ and NO are produced simultaneously, as it is presumed to occur in central nervous system. Indeed, the levels of nitrotyrosine, which is a product of the reaction of ONOO$^-$ with tyrosine residues and considered as a permanent footprint of ONOO$^-$, have been reported to increase in AD, PD and MS brains (Torreilles et al., 1999; Liu et al., 2001). Accordingly, the ONOO$^-$ forming blockers including PS/PC liposomes seem to be neuroprotective and a potentially useful treatment for these neurodegenerative diseases.

Due to the pivotal role of $^{\bullet}O_2^-$ in microglia-mediated neuroinflammation and oxidative stress, we employed ESR with the spin trap technique using DEPMPO to directly measure microglial $^{\bullet}O_2^-$ generation. The DEPMPO is an appropriate spin-trapping agent for cell-generated-$^{\bullet}O_2^-$ detection because of its stability and capability of differentiating between $^{\bullet}O_2^-$ and $^{\bullet}OH$ (Shi et al., 2005; Mojovic et al., 2005). LPS/PMA-activated microglia gave rise to ESR spectra consisting of a linear combination of $^{\bullet}O_2^-$ spin-adduct DEPMPO–OOH and spin-adduct DEPMPO–OH. Radical generation was totally quenched by SOD but not by catalase, thus indicating that H_2O_2, which is reduced to $^{\bullet}OH$ by Fenton reaction in the presence of Fe^{2+} or Zn^{2+}, was not a significant reactant in the formation of the observed radial signals. Moreover, the DEPMPO–OH appears to be generated by a spontaneous reduction of DEPMPO–OOH, not from H_2O_2-derived $^{\bullet}OH$ (Mojovic et al., 2005).

Colton et al. (1994) have reported that $^{\bullet}O_2^-$ and NO are apparently not produced by the same activating agent in rat primary cultured microglia. LPS is one of the most common stimulators used to activate microglia (O'Shea et al., 2006; Suuronen et al., 2006) both *in vivo* and *in vitro* models of neuroinflammation-mediated neurodegeneration and is known to activate protein–tyrosine kinases, mitogen-activated protein kinases (MAPKs) and nuclear factor-κB (NF-κB), which have been implicated in the release of NO and various pro-inflammatory cytokines (Rivest, 2003; Suuronen et al., 2006; Szelenyi et al., 2006). On the other hand, PMA assembles NADPH oxidase via activation of protein kinase C (PKC) and thus is commonly used to induce abrupt and large amounts of microglial $^{\bullet}O_2^-$ production called as respiratory burst. Although several studies have demonstrated that microglia activated by LPS can form $^{\bullet}O_2^-$ (Qin et al., 2004, 2005), our study demonstrated that LPS alone did not affect the microglial $^{\bullet}O_2^-$ production but it did induce NO production. In contrast, PMA alone induced microglial $^{\bullet}O_2^-$ generation without affecting the NO production. In addition, according to our findings, and consistent with the study by Colton et al., it is suggested that $^{\bullet}O_2^-$ and NO production are differentially regulated in cultured murine microglial cells. Namely, LPS appears to be an inflammogen that provokes microglial production of NO rather than $^{\bullet}O_2^-$. We cannot, however, eliminate the possibility that LPS stimulation mediates the pathway(s) associated with $^{\bullet}O_2^-$ generation in microglia,

because of differences on $^{\bullet}O_2^-$ detection sensitivity between the ESR assay and the other indirect methods.

We demonstrated that PS/PC liposomes considerably inhibited both the $^{\bullet}O_2^-$ and NO production in LPS/PMA-activated microglia, even though both of them appear to be regulated by distinct signal pathways. Furthermore, we also demonstrated that PS/PC liposomes did not scavenge $^{\bullet}O_2^-$, but instead act on the $^{\bullet}O_2^-$-generating system in microglia. The exact mechanism of PS/PC liposomes to suppress inflammatory activation of microglial has not yet been elucidated. Concerning $^{\bullet}O_2^-$ production, not only PS/PC liposomes but also PC liposomes inhibited the LPS/PMA-induced microglial production. Dipalmitoyl PC (DPPC), a kind of PC and the major component of pulmonary surfactant, has been shown to reduce monocyte respiratory burst via the downregulation of PKC associated with plasma membrane by the presumed mechanism that DPPC induces membrane perturbation (Tonks et al., 2005). In addition to that, according to our finding that few PC liposomes were phagocytosed by the micrglia, PC liposomes seem to act as membrane perturbers, thus reducing the LPS/PMA-induced and PKC-mediated $^{\bullet}O_2^-$ production. In contrast, PS has been reported to be engulfed by phagocytes through PS-recognizing receptor such as PS receptor (Fadok et al., 2000; De Simone et al., 2002) and scavenger receptor class B type 1 (Zhang et al., 2005). Indeed, it is confirmed that PS/PC liposomes could be phagocytosed by microglia in our study. However, we cannot rule out the possibility that PS/PC liposomes also induced the membrane perturbation under our experimental conditions because PS/PC liposomes contain 70 molar% PC. On the other hand, Ajmone-Cat et al. (2003) demonstrated that PS/PC-containing liposomes inhibited the phosphorylation of p38 MAPK and delayed that of cAMP responding element-binding protein in LPS-activated microglia. Because phosphorylation of p38 MAPK has been shown to mediate the signal pathway reacting for inflammatory stimulants and result in gene induction of NO synthase in microglia (Koistinaho and Koistinaho, 2002), the PS/PC liposomes-induced inhibition of p38 MAPK phosphorylation in activated microglia appears to suppress, at least partially, NO generation. In contrast, our finding that PC liposomes had no effect on LPS/PMA-induced NO production indicates that the presumed membrane perturbation induced by PC liposomes is not involved in NO-generating pathway(s) in the LPS/PMA-activated microglia.

Several neuroprotective compounds such as isoproterenol, dexamethasone, nicergoline, and naloxone have been shown to suppress microglial activation and thus decrease the ROS generation (Colton and Chernyshev, 1996; Yoshida et al., 2001; Qin et al., 2005). In comparison to the effective concentrations of these compounds (e.g. isoproterenol and nicergoline act at micromolar, naloxone acts even at femtomolar), the total lipids concentration such as millimolar of PS/PC liposomes used in this study seems to certainly be high. Borisenko et al. (2003), however, have suggested that phagocytes have a sensitivity threshold for PS externalized on the target cell surface, which thus provides for the reliable recognition and distinction between normal cells with low amounts of externalized PS and

apoptotic cells with remarkably elevated PS levels. They estimated that, using the liposomes containing PS and PC (1:1), the absolute amounts of PS required for phagocytosis by 5×10^4 macrophages (the threshold of macrophage sensitivity) was 7 pmol. This value of the PS amount for 10^6 macrophages (i.e. 140 pmol) approximates to the normalized value of the PS amount for 10^6 microglial cells, which was found to be considerably effective in our study (i.e. 75 pmol). Taken together, these findings suggest that microglia also require the relatively high phospholipids concentration to recognize PS/PC liposomes as apoptotic cells. Accordingly, new techniques to ameliorate the stability of PS/PC liposomes and thus reduce the effective phospholipids concentration are called for based on the findings of *in vivo* studies.

Acknowledgements

References

Ajmone-Cat, M.A., De Simone, R., Nicolini, A., Minghetti, L., 2003. Effects of phosphatidylserine on p38 mitogen activated protein kinase, cyclic AMP responding element binding protein and nuclear factor-kappa B activation in resting and activated microglial cells. J. Neurochem. 84, 413–416.

Beckman, J.S., 1994. Peroxynitrite versus hydroxyl radical: the role of nitric oxide in superoxide-dependent cerebral injury. Ann. N.Y. Acad. Sci. 738, 69–75.

Borisenko, G.G., Matsura, T., Liu, S.X., Tyurin, V.A., Jianfei, J., Serinkan, F.B., Kagan, V.E., 2003. Macrophage recognition of externalized phosphatidyl-serine and phagocytosis of apoptotic Jurkat cells—existence of a threshold. Arch. Biochem. Biophys. 413, 41–52.

Chang, R.C., Rota, C., Glover, R.E., Mason, R.P., Hong, J.S., 2000. A novel effect of an opioid receptor antagonist, naloxone, on the production of reactive oxygen species by microglia: a study by electron paramagnetic resonance spectroscopy. Brain Res. 854, 224–229.

Colton, C.A., Snell, J., Chernyshev, O., Gilvert, D.L., 1994. Induction of superoxide anion and nitric oxide production in cultured microglia. Ann. N.Y. Acad. Sci. 738, 54–63.

Colton, C.A., Chernyshev, O.N., 1996. Inhibition of microglial superoxide anion production by isoproterenol and dexamethasone. Neurochem. Int. 29, 43–53.

Combs, C.K., Karlo, J.C., Kao, S.C., Landreth, G.E., 2001. Beta-amyloid stimulation of microglia and monocytes results in TNF alpha-dependent expression of inducible nitric oxide synthase and neuronal apoptosis. J. Neurosci. 21, 1179–1188.

De Simone, R., Ajmone-Cat, M.A., Nicolini, A., Minghetti, L., 2002. Expression of phosphatidylserine receptor and down-regulation of pro-inflammatory molecule production by its natural ligand in rat microglial cultures. J. Neuropathol. Exp. Neurol. 61, 237–244.

Fadok, V.A., Voelker, D.R., Campbell, P.A., Cohen, J.J., Bratton, D.L., Henson, P.M., 1992. Exposure of phosphatidylserine on the surface of apoptotic lymphocytes triggers specific recognition and removal by macrophages. J. Immunol. 148, 2207–2216.

Fadok, V.A., Bratton, D.L., Konowal, A., Freed, P.W., Westcott, J.Y., Henson, P.M., 1998. Macrophages that have ingested apoptotic cells in vitro inhibit proinflammatory cytokine production through autocrine/paracrine mechan-isms involving TGF-beta, PGE2, and PAF. J. Clin. Invest. 101, 890–898.

Fadok, V.A., Bratton, D.L., Rose, D.M., Pearson, A., Ezekewitz, R.A., Henson, P.M., 2000. A receptor for phosphatidylserine-specific clearance of apoptotic cells. Nature 405, 85–90.

Hashioka, S., Monji, A., Ueda, T., Kanba, S., Nakanishi, H., 2005. Amyloid-beta fibril formation is not necessarily required for microglial activation by the peptides. Neurochem. Int. 47, 369–376.

Herrera-Molina, R., von Bernhardi, R., 2005. Transforming growth factor-beta 1 produced by hippocampal cells modulates microglial reactivity in culture. Neurobiol. Dis. 19, 229–236.

Kanzawa, T., Sawada, M., Kato, M., Yamamoto, K., Mori, H., Tanaka, R., 2000. Differentiated regulation of allo-antigen presentation by different types of murine microglial cell lines. J. Neurosci. Res. 62, 383–388.

Koistinaho, M., Koistinaho, J., 2002. Role of p38 and p44/42 mitogen-activated protein kinases in microglia. Glia 40, 175–183.

Li, J., Baud, O., Vartanian, T., Volpe, J.J., Rosenberg, P.A., 2005. Peroxynitrite generated by inducible nitric oxide synthase and NADPH oxidase mediates microglial toxicity to oligodendrocytes. Proc. Natl. Acad. Sci. U.S.A. 102, 9936–9941.

Liu, J.S., Zhao, M.L., Brosnan, C.F., Lee, S.C., 2001. Expression of inducible nitric oxide synthase and nitrotyrosine in multiple sclerosis lesions. Am. J. Pathol. 158, 2057–2066.

McGeer, P.L., Itagaki, S., Boyes, B.E., McGeer, E.G., 1988. Reactive microglia are positive for HLA-DR in the substantia nigra of Parkinson's and Alzheimer's disease brains. Neurology 38, 1285–1291.

McGeer, P.L., McGeer, E.G., 2002. Inflammatory processes in amyotrophic lateral sclerosis. Muscle Nerve 26, 459–470.

Meda, L., Cassatella, M.A., Szendrei, G.I., Otvos Jr., L., Baron, P., Villalba, M., Ferrari, D., Rossi, F., 1995. Activation of microglial cells by beta-amyloid protein and interferon-gamma. Nature 374, 647–650.

Mojovic, M., Vuletic, M., Bacic, G.G., 2005. Detection of oxygen-centered radicals using EPR spin-trap DEPMPO: the effect of oxygen. Ann. N.Y. Acad. Sci. 1048, 471–475.

Morris, R.H., Price, A.J., Tonks, A., Jackson, S.K., Jones, K.P., 2000. Pros-taglandin E2 and tumour necrosis factor-alpha release by monocytes are modulated by phospholipids. Cytokine 12, 1717–1719.

Navarro-Antolin, J., Lopez-Munoz, M.J., Soria, J., Lamas, S., 2002. Superoxide limits cyclosporine-A-induced formation of peroxynitrite in endothelial cells. Free Radic. Biol. Med. 32, 702–711.

Navikas, V., Link, H., 1996. Review: cytokines and the pathogenesis of multiple sclerosis. J. Neurosci. Res. 45, 322–333.

Nishikawa, K., Arai, H., Inoue, K., 1990. Scavenger receptor-mediated uptake and metabolism of lipid vesicles containing acidic phospholipids by mouse peritoneal macrophages. J. Biol. Chem. 265, 5226–5231.

Okada, M., Irie, S., Sawada, M., Urae, R., Urae, A., Iwata, N., Ozaki, N., Akazawa, H., Nakanishi, H., 2003. Pepstatin A induces extracellular acidification distinct from aspartic protease inhibition in microglial cell lines. Glia 43, 167–174.

O'Shea, R.D., Lau, C.L., Farso, M.C., Diwakarla, S., Zagami, C.J., Svend-sen, B.B., Feeney, S.J., Callaway, J.K., Jones, N.M., Pow, D.V., Danbolt, N.C., Jarrott, B., Beart, P.M., 2006. Effects of lipopolysaccharide on glial phenotype and activity of glutamate transporters: evidence for delayed up-regulation and redistribution of GLT-1. Neurochem. Int. 48, 604–610.

Possel, H., Noack, H., Keilhoff, G., Wolf, G., 2002. Life imaging of peroxynitrite in rat microglial and astroglial cells: role of superoxide and antioxidants. Glia 38, 339–350.

Qin, L., Liu, Y., Cooper, C., Liu, B., Wilson, B., Hong, J.S., 2002. Microglia enhance beta-amyloid peptide-induced toxicity in cortical and mesence-phalic neurons by producing reactive oxygen species. J. Neurochem. 83, 973–983.

Qin, L., Liu, Y., Wang, T., Wei, S.J., Block, M.L., Wilson, B., Liu, B., Hong, J.S., 2004. NADPH oxidase mediates lipopolysaccharide-induced neuro-toxicity and proinflammatory gene expression in activated microglia. J. Biol. Chem. 279, 1415–1421.

Qin, L., Block, M.L., Liu, Y., Bienstock, R.J., Pei, Z., Zhang, W., Wu, X., Wilson, B., Burka, T., Hong, J.S., 2005. Microglial NADPH oxidase is a novel target for femtomolar neuroprotection against oxidative stress. FASEB J. 19, 550–557.

Rivest, S., 2003. Molecular insights on the cerebral innate immune system. Brain Behav. Immunol. 17, 13–19.

Sankarapandi, S., Zweier, J.L., Mukherjee, G., Quinn, M.T., Huso, D.L., 1998. Measurement and characterization of superoxide generation in microglial cells: evidence for an NADPH oxidase-dependent pathway. Arch. Biochem. Biophys. 353, 312–321.

Shi, H., Timmins, G., Monske, M., Burdick, A., Kalyanaraman, B., Liu, Y., Clement, J.L., Burchiel, S., Liu, K.J., 2005. Evaluation of spin trapping agents and trapping conditions for detection of cell-generated reactive oxygen species. Arch. Biochem. Biophys. 437, 59–68.

Suuronen, T., Huuskonen, J., Nuutinen, T., Salminen, A., 2006. Characterization of the pro-inflammatory signaling induced by protein acetylation in microglia. Neurochem. Int. 49, 610–618.

Szelenyi, J., Selmeczy, Z., Brozik, A., Medgyesi, D., Magocsi, M., 2006. Dual beta-adrenergic modulation in the immune system: stimulus-dependent effect of isoproterenol on MAPK activation and inflammatory mediator production in macrophages. Neurochem. Int. 49, 94–103.

Tanaka, M., Sotomatsu, A., Yoshida, T., Hirai, S., Nishida, A., 1994. Detection of superoxide production by activated microglia using a sensitive and specific chemiluminescence assay and microglia-mediated PC12h cell death. J. Neurochem. 63, 266–270.

Tonks, A., Parton, J., Tonks, A.J., Morris, R.H., Finall, A., Jones, K.P., Jackson, S.K., 2005. Surfactant phospholipid DPPC downregulates monocyte respiratory burst via modulation of PKC. Am. J. Physiol. Lung Cell Mol. Physiol. 288, L1070–L1080.

Torreilles, F., Salman-Tabcheh, S., Guerin, M., Torreilles, J., 1999. Neurodegenerative disorders: the role of peroxynitrite. Brain Res. Rev. 30, 153–163.

Xie, Z., Wei, M., Morgan, T.E., Fabrizio, P., Han, D., Finch, C.E., Longo, V.D., 2002. Peroxynitrite mediates neurotoxicity of amyloid beta-peptide 1-42 and lipopolysaccharide-activated microglia. J. Neurosci. 22, 3484–3492.

Yoshida, T., Tanaka, M., Okamoto, K., 2001. Inhibitory effect of nicergoline on superoxide generation by activated rat microglias measured using a simple chemiluminescence method. Neurosci. Lett. 297, 5–8.

Zhang, J., Fujii, S., Wu, Z., Hashioka, S., Tanaka, Y., Shiratsuchi, A., Nakanishi, Y., Nakanishi, H., 2005. Involvement of COX-1 and up-regulated prostaglandin E synthases in phosphatidylserine liposome-induced prostaglandin E2 production by microglia. J. Neuroimmunol. 172, 112–120.

Neuroprotective effect of exogenous microglia in global brain ischemia

Fumihiro Imai[1], Hiromi Suzuki[2], Jumpei Oda[1], Takashi Ninomiya[1], Kenji Ono[2], Hirotoshi Sano[1] and Makoto Sawada[2]

[1]Department of Neurosurgery, Fujita Health University, Toyoake, Aichi, Japan; [2]Department of Brain Life Science, Research Institute of Environmental Medicine, Nagoya University, Furo-cho, Chikusa-ku, Nagoya, Aichi, Japan

Exogenous microglia pass through the blood–brain barrier and migrate to ischemic hippocampal lesions when injected into the circulation. We investigated the effect of exogenous microglia on ischemic CA1 pyramidal neurons. Microglia were isolated from neonatal mixed brain cultures, labeled with the fluorescent dye PKH26, and injected into the subclavian artery of Mongolian gerbils subjected to ischemia reperfusion neuronal injury. PKH26-labeled microglia migrated to the ischemic hippocampal lesion, resulting in increased numbers of surviving neurons compared with control animals, even when injected 24 h after ischemia. Interferon-γ stimulation of isolated microglia enhanced the neuroprotective effect. Administration of exogenous microglia resulted in normal performance in a passive avoidance-learning task. Additionally, administration of exogenous microglia increased the expression of brain-derived neurotrophic factor and glial cell line-derived neurotrophic factor in the ischemic hippocampus, and thus might have induced neurotrophin-dependent protective activity in damaged neurons. Peripherally injected microglia exhibited a specific affinity for ischemic brain lesions, and protected against ischemic neuronal injury in vivo. It is possible that administration of exogenous microglia can be developed as a potential candidate therapy for central nervous system repair after transitory global ischemia.
Journal of Cerebral Blood Flow & Metabolism (2007) 27, 488–500. doi:10.1038/sj.jcbfm.9600362; published online 5 July 2006

Introduction

Microglia arise from the monocyte/macrophage lineage, and are ubiquitously distributed in the central nervous system, representing up to 20% of the total glial cell population in the brain (Lawson et al, 1990). In accordance with del Rio Hortega's early teaching (Hortega, 1932), the current view is that resident microglia are of mesodermal origin, derived from bone marrow precursor cells (Ling and Wong, 1993). These cells invade the central nervous system at an early embryonic stage to give rise to typical process-bearing microglia (Ling and Wong, 1993). Therefore, microglia may have high affinity for the brain.

Many reports describe neuron–microglia interactions after cerebral ischemia and mechanical injury (for review, see Gehrmann et al, 1995). It remains controversial, however, whether activated microglia promote neuronal death or neuronal survival. Many investigators maintain that microglia induce a neurotoxic effect by secreting nitric oxide (Chao et al, 1992) and toxic cytokines (Sawada et al, 1989). Moreover, microglia may contribute to the pathogenesis of neurodegeneration, such as in multiple sclerosis (Diemel et al, 1998), Alzheimer's disease (Barger and Harmon, 1997), and acquired immunodeficiency syndrome-associated dementia (Giulian et al, 1996). Conversely, other studies show that microglia protect neurons in the damaged brain by secreting cytokines, such as interleukin-1β (Giulian et al, 1986), interleukin-6 (Sawada et al, 1995), transforming growth factor-β (Suzumura et al, 1993),

basic fibroblast growth factor (Shimojo *et al*, 1991), hepatocyte growth factor (Hamanoue *et al*, 1996), nerve growth factor (Mallat *et al*, 1989), and tumor necrosis factor α (Sawada *et al*, 1989).

To determine whether microglia are neurotoxic or neuroprotective, they must be analyzed with *in vivo* models of neuronal injury. The role of microglia may be clarified by injecting isolated microglia at the site of neuronal injury in animal models. Direct injection of microglia into the brain, however, induces undesirable events, such as the entry of blood cells to the site of injury and immunologic responses, which complicate the analysis of the role of microglia.

Our previous studies showed that microglia isolated from rodent mixed-brain cultures retain the ability to enter the normal brain from the circulation (Imai *et al*, 1997, 1999; Sawada *et al*, 1998). Hence, microglia can be introduced into the central nervous system by injection into the bloodstream in animal models of neuronal injury. Using this system, the roles of microglia in various pathologic conditions can be analyzed.

The purpose of the present study was to evaluate whether microglia have neurotrophic or neurotoxic effects on *in vivo* brain ischemia, in which CA1 pyramidal neurons are specifically damaged. Microglia isolated from a primary culture of mixed glial cells from neonatal Mongolian gerbils were injected into the subclavian arteries of host animals subjected to ischemia reperfusion neuronal injury. We examined the number of CA1 pyramidal neurons in the brain at various time points up to 8 days. In another group of animals, we tested the effect of microglia injection on performance in a passive avoidance-learning task. We also investigated changes in the expression of brain-derived neurotrophic factor (BDNF) and glial cell line-derived neurotrophic factor (GDNF) in the ischemic hippocampus after microglia injection.

Materials and methods

Animals and Induction of Global Forebrain Ischemia

Adult male Mongolian gerbils (*n* = 300; 7 to 8 weeks old; ≈60 g; Seac Yoshitomi, Ltd, Fukuoka, Japan) were used in the study. Animals were housed individually, with food and water available *ad libitum*. All procedures were performed in accordance with the Guidelines for Animal Experimentation of the Fujita Health University, School of Medicine.

Ischemia was induced as described by Tone *et al* (1987). In brief, anesthesia was induced and maintained with a mixture of 2.5% halothane and nitrous oxide/oxygen (1:1). Body temperature was maintained at 37°C with a heating pad. When the spinal reflex was absent, both common carotid arteries were exposed through a ventral cervical incision and occluded with aneurysm clips for 5 mins. The clips were then released to resume normal flow to the forebrain (ISCH). Gerbils operated on without occlusion of

the carotid arteries were used as controls (sham ISCH). Postoperative rectal temperature was measured three times daily (at 0700, 1400, and 2200) immediately after the induction of anesthesia with a mixture of 2.5% halothane and nitrous oxide/oxygen (1:1).

Duration of Survival Period

Ischemia was confirmed by examination of Nissl-stained brain sections 7 days after ischemia. Delayed neuronal death was observed in CA1 pyramidal neurons in all animals (*n* = 20). Approximately 2% of the animals did not survive the ischemic episode. All animals that survived were included in the data analysis. There were no differences in survival between groups.

Cell Culture

Microglia were prepared using postnatal day 1 Mongolian gerbils (*n* = 200), as described previously (Suzumura *et al*, 1984). In brief, the meninges were removed, and the brain was dissociated by passing it through a 320-μm-pore nylon mesh. After washing with Hank's balanced salt solution, the cell suspension was triturated and plated in 75-cm^2 culture flasks (Falcon 3024, Becton-Dickinson, Franklin Lakes, NJ, USA) at a density of one brain per flask in 10 mL Eagle's minimal essential medium, supplemented with 10% fetal bovine serum, 5 μg/mL bovine insulin, and 0.2% glucose. Microglia were isolated on the 14th day by the shaking off method (Suzumura *et al*, 1984). In some experiments, purified microglia were stimulated by incubation with human interferon-γ (IFNγ; Shionogi Co., Osaka, Japan) at a concentration of 5 × 10^3 U in 10 mL in a plastic dish at 37°C for 24 h.

Macrophages were collected by injecting 10 mL of cold (4°C) phosphate-buffered saline into the peritoneal cavities of a separate group of gerbils. Peritoneal fluid was withdrawn three times with a 21-gauge needle attached to a plastic syringe. The cells were maintained at 4°C, centrifuged at 1,000 *g* for 5 mins, and seeded onto plastic dishes containing Eagle's minimal essential medium with 10% fetal bovine serum, where they adhered for 1 h at 37°C in 5% CO_2.

PKH26 Labeling

PKH staining provides stable, clear, intense, accurate, and reproducible fluorescent labeling of live cells for an extended period of time, with no apparent toxic effects (Horan and Slezak, 1989). PKH is an aliphatic reporter molecule that is inserted into the cell membrane lipid bilayer by selective partitioning. It is effective for a variety of cell types and exhibits no significant leaking or transfer between cells. We used PKH26 to label the exogenous microglia within the brain, using a PKH26 Red Fluorescent Cell Linker Kit for Phagocytic Cell Labeling (PKH26-PCL; Sigma Chemical Co., St Louis, MO, USA). PKH26-PCL labels phagocytic cells with excitation (551 nm) and emission (567 nm) wavelengths compatible

with rhodamine or phycoerythrin detection systems. The labeling occurs through the formation of aggregates of particles. The aggregation significantly inhibits the uptake of dye by nonphagocytic cells, such as lymphocytes, but facilitates dye uptake by phagocytic cells. Labeled cells appear patchy or spotted because the dye localizes in phagocytic compartments of the cells. The dye appears to be resistant to metabolic breakdown and labels the cells for at least 21 days in vivo. Use of PKH26 can be combined with immunocytochemistry (Silverman et al, 2000), but is not suitable for double staining, because it is easily abolished by the fixation required for immunocytochemistry.

Labeling of microglia and macrophages with PKH26 was performed using the standard phagocytosis procedure of microscopic particles, according to the manufacturer's instructions. In brief, cells in a 10-cm plastic dish were incubated with PKH26 staining solution containing 10 μmol/L PKH26, 50% Diluent B (a phagocytic cell-labeling solution, Sigma Chemical Co.), and 50% culture medium for 15 mins, then washed three times in 10 mL of serum-containing medium. PKH26-stained cells were harvested using a rubber policeman in 2 mL of ice-cold phosphate-buffered saline (pH 7.2) and washed three times with 5 mL of ice-cold phosphate-buffered saline (pH 7.2) by centrifugation at 1,000 g for 3 mins. The cells were then resuspended in the culture medium for injection into the host.

Injection of Cells

Intraarterial cell injection was performed as described previously (Ishihara et al, 1993). Cells were injected either 24 h before or 24 h after ischemia was induced. In a subset of experiments, microglia were injected 48 h after ischemia induction. In brief, sham ISCH and ISCH gerbils were anesthetized with a mixture of 2.5% halothane and nitrous oxide/oxygen (1:1). When the spinal reflex was absent, a transverse incision was made under the left clavicle. The left subclavian artery was exposed and dissected from the surrounding tissues. After temporary occlusion of the subclavian artery with an aneurysm clip, a small hole was made in the distal side of the artery with a 27-gauge needle, and a polyethylene tube (Becton Dickinson, Tokyo, Japan) was inserted proximally into the hole. After the aneurysm clip was released, PKH26-labeled microglia or macrophages (0.5 mL of final suspension media estimated to contain 1×10^6 cells) were injected as a bolus for 30 secs into the subclavian artery through the polyethylene tube.

Tissue Preparation

Gerbils were deeply anesthetized with ketamine hydrochloride (60 mg/kg, intraperitoneally) and killed by transcardial perfusion with isotonic saline solution. Brains were removed, frozen in liquid nitrogen, and embedded in OTC compound (Tissue Tek, Elkhart, IN, USA). Coronal sections (8 μm thick) at the hippocampal level were cut with a cryostat, mounted on slides, and dried. To preserve

PKH26 labeling, the sections were lightly fixed with 4% paraformaldehyde in 0.1 mol/L phosphate buffer, pH 7.2, for 10 mins. To determine the location of exogenous microglia relative to ischemic CA1 pyramidal neurons, an immunofluorescent study was performed using terminal deoxynucleotidyl transferase (TdT)-mediated deoxyuracil nucleotides-biotin nick-end labeling (TUNEL), Griffonia simplifolia B4 isolectin (IB4), and an antibody to microtubule-associated protein 2 (MAP2). To localize BDNF and GDNF expression, immunohistochemistry using the avidin–biotin complex method was performed.

TUNEL staining was used to detect DNA fragmentation in cell nuclei. The hippocampal sections were pretreated with or without 20 μg/mL proteinase K (Sigma Chemical Co.) at room temperature (RT) for 15 mins. After treatment with 0.3% H_2O_2 in methanol for 30 mins, sections were incubated with 100 U/mL TdT and 10 nmol/L per mL biotinylated 16-2′-dUTP (Boehringer-Mannheim-Yamanouchi, Tokyo, Japan) in TdT buffer (100 mmol/L sodium cacodylate, pH 7.0, 1 mmol/L cobalt chloride, and 50 μg/mL gelatin) in a humid atmosphere at 37°C for 60 mins. Further incubation with fluorescein isothiocyanate-conjugated avidin (Nichirei, Tokyo, Japan) was performed for 60 mins at RT.

Microglial cells were identified by IB4 staining. Cryosections were incubated with 20 μg/mL biotinylated IB4-fluorescein isothiocyanate conjugate (Sigma Chemical Co.) in 0.01 mol/L phosphate-buffered 0.15 mol/L saline (pH 7.2) containing 0.1% Triton X-100 at RT for 2 h (Streit, 1990).

Hippocampal CA1 pyramidal neurons were visualized using a monoclonal antibody to MAP2 (Chemicon, Temecula, CA, USA). Sections were incubated with 10% normal goat serum for 30 mins at RT. They were then incubated with a mouse monoclonal anti-MAP2 antibody, diluted 1:100, for 1 day at 4°C. Further incubations were performed with fluorescein isothiocyanate-conjugated anti-mouse IgG (Jackson ImmunoResearch Laboratories, West Grove, PA, USA), diluted 1:500, at RT for 60 mins.

We visualized BDNF epitopes using a rabbit polyclonal anti-BDNF antibody (diluted 1:500; Santa Cruz Biotechnology, Santa Cruz, CA, USA) and GDNF epitopes were visualized using a rabbit polyclonal anti-GDNF antibody (diluted 1:250; Santa Cruz Biotechnology). Sections were then incubated in secondary antibody, biotinylated goat anti-rabbit IgG, followed by avidin–biotin complex (Elite kit: Vector Laboratories, Burlingame, CA, USA), and visualized after chromogenic reaction with 3,3′-diaminobenzidine.

The sections were analyzed with an Olympus BX51 microscope equipped with bright-field and fluorescent light sources (Tokyo, Japan). Both bright-field and fluorescent images were captured from the same field using a Penguin 600 CL camera (Pixera Corporation, Los Gatos, CA, USA).

Cell Counts

Six serial, coronal frozen sections (8 μm thick) at the CA1 hippocampal level were examined. Cells were counted if

they were within a randomly selected 1-mm linear length of CA1. To determine the time course of exogenous microglia migration to the ischemic hippocampus, PKH26-labeled microglia were counted in animals injected with nonstimulated or IFNγ-stimulated microglia 24 h before ischemia, and at 2, 3, 5, and 7 days after ischemia. To determine whether exogenous microglia reduced ischemic damage caused by transient global ischemia, surviving pyramidal neurons were counted in ISCH or sham ISCH animals infused with vehicle (ISCH/ VEH, SHAM/VEH), nonstimulated microglia (ISCH/Mi, SHAM/Mi), or IFNγ-stimulated microglia (ISCH/γMi, SHAM/γMi), 24 h before (PRE) or 24 h after (POST) ischemia. All neurons (cresyl violet-positive cells) with an intact morphologic appearance were counted in each animal either 7 or 14 days after ischemia. A total of 10 animals were examined for each of the 12 conditions.

Passive Avoidance Task

A step-through type passive avoidance apparatus was used to evaluate memory, as described previously (Nanri et al, 1998). The apparatus comprised two compartments: one light and one dark (each 16.5 × 16.0 × 14.7 cm), separated by a guillotine door. The dark compartment had a stainless-steel grid floor. A scrambled electric shock was delivered through the grid floor by a shock generator (Daiichi Kikai Inc., Tokushima, Japan). The passive avoidance learning trial was performed either 7 or 14 days after inducing ischemia. At the beginning of the training session, each animal was placed in the light compartment. When the animal stepped into the dark compartment, the door between compartments was closed and a foot shock (0.6 mA, 3 secs) was delivered through the floor. The door was then opened and the animal was allowed to cross back into the light compartment. Each time the animal stepped into the dark compartment, a foot shock was delivered. Eventually, the animal remained in the light compartment. The learning trial lasted 8 mins.

The retention test was performed 24 h after the learning trial. In the retention test, the gerbil was placed in the light compartment, and the latency to enter the dark compartment was measured. If the gerbil did not enter the dark compartment within 180 secs, a score of 180 secs was assigned. Performance on the passive avoidance task was evaluated in the SHAM/VEH-(PRE/POST), ISCH/VEH-(PRE/POST), ISCH/Mi-(PRE/POST), and ISCH/γMi-(PRE/ POST) groups. Ten animals were used for each of the eight conditions.

Enzyme-Linked Immunosorbent Assay

Changes in BDNF and GDNF levels were measured in the hippocampus in SHAM/VEH, ISCH/VEH, ISCH/Mi, or ISCH/γMi animals using the BDNF and GDNF Emax Immunoassay System Kit (Promega, Madison, WI, USA). In the hippocampus of ISCH/VEH-PRE or ISCH/Mi-PRE gerbils, each neurotrophic factor level was measured 2 h, 1 day, 3 days, and 7 days after inducing ischemia. In the hippocampus of ISCH/VEH-POST and ISCH/Mi-POST

animals, each neurotrophic factor level was measured 26 h, 2 days, 4 days, and 8 days after ischemia. As a control, we used the hippocampus from SHAM/VEH-PRE animals, which was dissected 6 h after the treatment (Marmigere et al, 2003). Neurotrophic factor levels were also measured in the rest of the brain after the hippocampus was removed.

Results

Recruitment of Exogenous Microglia into CA1 Hippocampal Lesions

Figure 1 shows fluorescent staining in the hippocampal CA1 field of ISCH animals injected with PKH26-labeled exogenous microglia 24 h before ischemia. PKH26-labeled cells accumulated near TUNEL-positive cells (Figures 1A–1D). PKH26-labeled cells were also located in the vicinity of MAP2-positive pyramidal neurons 3 days after ischemia (Figure 2A). IB4 staining of adjacent sections revealed that all PKH26-labeled cells were IB4-positive (Figures 2B–2D).

PKH26-labeled cells that reacted with IB4 were identified as microglia. Most of the microglia that accumulated in the CA1 field were both PKH26- and IB4-positive exogenous microglia, whereas there were only a few PKH26-negative and IB4-positive endogenous microglia (Figures 2B–2D). The TUNEL-positive cells were probably pyramidal neurons, because they were in the CA1 pyramidal cell layer and were not labeled with PKH26 (Figures 1A–1D). Neither TUNEL-positive pyramidal neurons nor PKH26-labeled microglia were detected in CA1 1 day after ischemia (data not shown). Two days after ischemia, only a few TUNEL-positive pyramidal neurons were detected in a portion of CA1, and PKH26-labeled microglia had accumulated in or around the TUNEL-positive neurons (Figures 1A and 1B). Three days after ischemia, a few TUNEL-positive pyramidal neurons were detected in CA1 (data not shown) and PKH26-labeled microglia were scattered throughout the CA1 field (Figure 2A). Five days after ischemia, many TUNEL-positive pyramidal neurons and PKH26-labeled microglia were distributed throughout CA1. Many of these cells had accumulated near the CA1–CA2 border (Figures 1C and 1D). The number of TUNEL-positive pyramidal neurons and PKH26-labeled microglia in the CA1 layer increased in a time-dependent manner until 7 days after ischemia (Figures 1A–1D and 3A). Stimulation with IFNγ increased the number of migrating exogenous microglia in the ischemic CA1 pyramidal cell layer (Figure 3A). The temporal profile of exogenous microglia recruitment was the same if the microglia were injected after ischemia onset (data not shown). In a separate set of experiments, PKH26-labeled macrophages did not enter the brain from the circulation (data not shown).